Mare Domes in Mare Tranquillitatis: Identification, Characterization, and Implications for Their Origin

Le Qiao[1], James W. Head[2], Lionel Wilson[3], Jian Chen[1], Zongcheng Ling[1]

[1]Shandong Key Laboratory of Optical Astronomy and Solar-Terrestrial Environment, School of Space Science and Physics, Institute of Space Sciences, Shandong University, Weihai, Shandong, 264209, China.

[2]Department of Earth, Environmental and Planetary Sciences, Brown University, Providence, RI 02912, USA.

[3]Lancaster Environment Centre, Lancaster University, Lancaster LA1 4YQ, UK.

Corresponding authors: Le Qiao (leqiao.geo@gmail.com)

Key Points:

- The distribution of over 200 mare domes in Mare Tranquillitatis shows a concentration in a broad rise in eastern Tranquillitatis
- The broad volcanic rise was formed by shield plains volcanism, differing from volcanism in younger mascon basins
- Differences between Mare Tranquillitatis and younger maria are due to greater ages of the basin and mare, and a shallower source region

Abstract

Mare domes, small shield volcanoes typically <~30 km diameter, are part of the spectrum of lunar volcanic features that characterize extrusive basalt deposits. We used new spacecraft data to document these in Mare Tranquillitatis, among the oldest maria and the site commonly interpreted as an ancient degraded non-mascon impact basin. We found 283 known and suspected mare domes, with the majority (n = 229) concentrated on a broad, ~450 km circular topographic rise in eastern Mare Tranquillitatis. The domes (median diameter 5.6 km, height 68 m, volume 0.7 km^3) contain summit pits (74%; median diameter 0.8 km), and exhibit minor compositional variability between domes and surrounding flows, suggesting that domes both supply and are embayed by these flows. Based on their characteristics and associations, we interpret the small shield volcanoes to have been built from individual low-volume (<~10–100 km^3), low volatile content, short duration, cooling-limited eruptions. The ~450 km *broad volcanic rise* is ~920 m high (volume ~1.6×10^5 km^3) and is interpreted to be built from multiple occurrences of small shield eruptions, a *shield plains volcanism* style. This implies a shallow mantle source region capable of supplying distributed dike-emplacement and eruption events over an area of 1.75×10^5 km^2 early in mare volcanism history (~3.7 Ga). The difference between Mare Tranquillitatis and younger mare-filled mascon basins is attributed to the more ancient thermal state and crustal structure of the viscously relaxed Tranquillitatis basin, and a shallower broad magma source region present in earlier lunar thermal history.

Plain Language Summary

Lunar mare volcanic activity spans several billion years in early-middle lunar history and involves melting in the mantle, ascent in blade-like cracks (dikes) and eruption to the surface to form basaltic lava flows. The features surrounding the eruption vent (e.g., flows, channels, sinuous rilles, cones, domes, pyroclastics, etc.) provide important information about eruption conditions (e.g., magma volume, rate of eruption, cooling behavior, composition, volatile content, etc.). The array of these features in specific mare locations and with differing ages provides critical information on the evolution of mantle source regions and the thermal evolution of the Moon. We studied ~3.7 Ga-aged lava deposits in Mare Tranquillitatis and found over 200 small shield volcanoes clustered in a ~450 km *broad volcanic rise*, and formed from a series of eruptions in a distinctive *shield plains volcanism* style. Missing or rare were other types of volcanic features (sinuous rilles, steep flow fronts, pyroclastics, cones, lava channels). Individual small shield volcanos are interpreted to have formed from relatively low-volume, low-volatile content, short-duration, cooling-limited eruptions. This unusual concentration in eastern Mare Tranquillitatis implies broad, relatively shallow source regions below this possible ancient, non-mascon impact basin, in contrast to later mascon-basin maria (Crisium, Serenitatis, Imbrium).

1. Introduction

Volcanism is one of the major geological process on the Moon, directly reflecting the composition and thermal state of the lunar interior and its evolution, and it serves as an important window into the geological and thermal evolution of the Moon. Investigation of the spatial distribution and characteristics of the resultant volcanic deposits can provide fundamental evidence for constraining eruption processes (style, mechanism, flux), magma composition (especially volatile species and contents) and physical properties, and the nature of magma source regions and their evolution (e.g., Head et al., 1981; Shearer et al., 2006; National Research Council, 2007; Spudis, 2015).

Mare domes, small (diameter mostly less than ~30 km) and generally circular structures with convex-upward profiles (Head & Gifford, 1980), are among the most common volcanic landforms on the Moon (Head & Wilson, 2017). Mare domes usually have very gentle slopes (generally less than 5°, many even <1°) and summit pit craters are often observed. Several hundred mare domes have been previously identified, mainly from telescope and orbital photographs (e.g., Head & Gifford, 1980; Wöhler et al., 2006, 2007; Tye & Head, 2013). However, due to their low topographic slopes, many of them can only be detected from images obtained at very low Sun illumination (for example near-terminator and in Earthshine; Head & Lloyd, 1971; Lloyd & Head, 1972), on which the shadows are long and the features are more apparent, thus enhancing detectability and morphologic identification. However, it is often very difficult to obtain very low-Sun spacecraft images for various reasons, including the very few illuminated areas under very low Sun elevations due to massive shadows and the requirement of long exposure time, off-nadir slews of orbital spacecraft, sophisticated panning of cameras and cumbersome data processing. Telescopic observation can obtain images of the lunar surface under very low Sun conditions, but the effective ground resolution is generally coarser than ~1 km due to atmospheric effects, making it very challenging for identifying smaller mare dome features (Lena et al., 2007; Kreslavsky et al., 2017).

Newly-obtained global high-resolution and high-precision lunar topographic data, for instance, the Kaguya/SELENE-TC (Terrain Camera) + LRO-LOLA (Lunar Orbiter Laser Altimeter) merged topography (SLDEM2015) with ~60 m spatial sampling and ~3–4 m vertical altimetric accuracy (Barker et al., 2016), provide an unprecedented tool for identifying and characterizing low-amplitude gently-sloping geomorphic features on the Moon, including mare domes. These data sets provide direct altimetric measurements of lunar surface topographic relief, enabling straightforward identification of geological features on the Moon, rather than geomorphologic interpretations from optical imagery via shadow patterns and albedo variations. Compared with conventional low-Sun image-based investigations, topographic data-based geological interpretations are free of illumination condition variations, imperfect mosaicking and the resultant potentially biased interpretation results.

The origin of lunar mare domes has been investigated by many authors and several formation mechanisms have been proposed. On the basis of many prior investigations and an improved knowledge of lunar geology in general (especially water content in lunar basalts), mare domes are generally regarded as magmatic in origin, and many other scenarios have been largely ruled out (e.g., partial degassing of lunar interior and gigantic bubbles beneath the surface, and serpentinization of olivine; Salisbury, 1961; Spurr, 1945). Many investigators interpreted lunar domes to be analogues to small terrestrial shield volcanoes and to be built up through multiple phases of flows erupted from a common pit crater source, dominated by accumulating low-effusion rate, cooling-limited flows (e.g., Head & Wilson, 2017, and references therein), though other formation mechanisms have also been proposed, for instance, laccolithic intrusions (e.g., Wöhler et al., 2007).

We initiated a global search campaign for mare domes, plotting their distribution, modes of occurrence, local and regional clustering, range of characteristics (diameter, height, shape, presence of pit craters, etc.) and associations (terrain, volcanic, structural, mineralogy, and age). As the first step of this project, we focused on Mare Tranquillitatis, which has one of the greatest concentrations of mare domes on the Moon (e.g., Head & Gifford, 1980; Tye & Head, 2013) and is an area identified by Spudis et al. (2013) as a potential large lunar shield volcano. In this analysis, we assess the characteristics, distribution and origin of mare domes in Mare Tranquillitatis, analyze hypotheses for their origin, place the population into the context of the generation, ascent, and eruption of basalt magma on the Moon (e.g., Wilson & Head, 2017a) and lunar geologic and thermal evolution (e.g., Shearer et al., 2006; Wieczorek et al., 2006).

2. Data and Methodology

We first employ the SLDEM2015 topography (Barker et al., 2016), with assistance from other multi-source altimetric (including the Kaguya TC stereogrammetry digital terrain model (DTM) (10 m spatial sampling size and ~3–4 m altimetric accuracy; Haruyama et al., 2012) and LRO LOLA Gridded Data Record (1024 pixel/degree; Smith et al., 2010)) and imaging (including LRO Wide-Angle Camera (LROC WAC, 100 m/pixel, Robinson et al., 2010) and Kaguya TC (10 m pixel size; Haruyama et al., 2008) low-Sun mosaics) data sets to (1) evaluate each mare dome identified in previous investigations and (2) search for new mare dome features in Mare Tranquillitatis. The SLDEM2015 and other topography data are represented as color-coded images with variable stretches using statistics from the local surface studied (for instance, a potential mare dome and its adjacent mare), not the entire extent of the data. This manner of topographic representation can maximize the available color ranges for each local area studied, because the human eye can easily distinguish many different colors more readily than many shades of a certain color, thus facilitating the identification of many gently-sloping mare dome features.

We delineate the base outline of each identified mare dome from color-coded topography and optical images. We then characterize the detailed morphology, morphometry, and topography of each catalogued mare dome using SLDEM2015 topography and TC low-Sun images, including dome base diameter, dome height, flank slope, dome volume, shape outline, cross-sectional topographic profiles, presence and nature (shape, size, depth, volume, etc.) of summit pit features, and associated volcanic features (including pyroclastic deposits, volcanic cones, lava flow fronts, sinuous rilles, irregular mare patches (IMPs), ring-moat dome structures (RMDSs), floor-fractured craters (FFCs), etc.). We also investigate the iron and titanium elemental abundances of these domes and the surrounding maria using FeO content maps calculated from Clementine Ultraviolet-Visible (UVVIS) data (100 m/pixel) and algorithms of Lucey et al. (2000) (1σ = ~1 wt.%), and TiO_2 content maps derived from LROC WAC multi-band reflectance (Sato et al., 2017; 400 m/pixel, $1\sigma < 0.3$ wt. % offset from Lunar Prospector TiO_2 contents for Mare Tranquillitatis), respectively. We do not use Kaguya Multiband Imager (MI) spectrometer data to study the chemical composition of Mare Tranquillitatis domes as the MI data set has relatively poor coverage in Mare Tranquillitatis, despite its higher spatial resolution (20 m/pixel; Otake et al., 2012). The ages of the background mare units of each dome are also catalogued from dating results calculated by the impact crater size-frequency distribution (CSFD) method (Hiesinger, Head, et al., 2011).

3. Geologic Setting of Mare Tranquillitatis: The Oldest Mare on the Moon

As the landing target of the first human exploration mission to the Moon, NASA's Apollo 11 in 1969, Mare Tranquillitatis is one of the best-studied maria on the Moon (Figures 1A and 1B). Apollo 11 collected and returned 22 kg of lunar samples from the southwestern edge of Mare Tranquillitatis, testifying to its unique importance in geologic studies of the Moon in various aspects, including characterizing mare volcanism and "ground-truthing" telescopic and orbital observations of the lunar surface.

The Tranquillitatis basin, the impact basin whose interior floor had been flooded by Mare Tranquillitatis basalts, has irregular outlines and lacks the well-defined, concentric topographic rings typical for many impact basins on the Moon (Figure 1B; although a recent global analysis of lunar basins by Neumann et al. (2015) found that Tranquillitatis did not meet their criteria as a basin of impact origin). Its degraded topographic and morphologic signature has been attributed to the intersection and overlap of rims of surrounding relatively younger basins (including Serenitatis, Crisium, Fecunditatis, Nectaris; De Hon, 2017) and significant viscous relaxation (Solomon et al., 1982). Previous photogeologic studies had designated it as a pre-Nectarian-aged basin (Wilhelms, 1987) with a main ring measuring 700 km in diameter (Spudis, 1993). A possible outer ring with an estimated diameter of 950 km, while poorly discernable, had also been interpreted (Spudis, 1993). These unusual characteristics led to the hypothesis of two overlapping basins (De Hon, 2017). Tranquillitatis basin is also distinctive in being a non-mascon basin: no basin-scale gravity anomalies (mass concentrations or mascons) are observed within the basin interior (Zuber et al., 2013). However, one local positive Bouguer anomaly with a diameter of ~200 km occurs at the Lamont ridge-ring structure in western Mare Tranquillitatis, interpreted to be either a buried igneous intrusion (Dvorak & Phillips, 1979) or a buried 370 km-diameter impact basin (Dvorak and Phillips, 1979; Neumann et al., 2015). In addition, another impact basin, Asperitatis, with an estimated main ring diameter of 730 km, has also been revealed in the southern part of the Tranquillitatis basin by gravity analyses (Neumann et al., 2015).

By measuring the diameter and rim height of partially buried impact craters, De Hon (1974) estimated the infilled mare basalts within Mare Tranquillitatis to be 500–600 m thick on average. The thickest basalts occur in a broad arc-shaped area between craters Lamont and Jansen in western Mare Tranquillitatis, with a projected thickness of 1740 m. However, an updated analysis incorporating a new crater shape model and topographic degradation process (Du et al., 2019) yielded a median thickness of ~25 m for Mare Tranquillitatis basalts (2–218 m range, from measurements at eight craters), over one order of magnitudes thinner than De Hon's result.

Mare Tranquillitatis is distinctive in its compositional characteristics of the mare basalt fill. Preliminary chemical analyses of the returned Apollo 11 basalt samples found that one of the most striking compositional characteristics of lunar basalts in comparison with terrestrial basalts is the unusually high concentration of titanium (7–12.5 wt. % TiO_2; LSPET, 1969). Post-Apollo telescopic spectral studies revealed that Mare Tranquillitatis contained some of the most titanium-rich basalts within the lunar nearside maria (HDWA basalts; Pieters, 1978). Staid et al. (1996) conducted spectral mixing analysis of Galileo multi-band images and estimated titanium abundances up to 8–10 wt.% TiO_2 for Tranquillitatis basalts. Global high-resolution multispectral mapping from Clementine enabled quantitative geochemical analyses of the lunar surface at the global scale. Lucey et al. (1998, 2000) established mathematic relationships between Clementine angular spectral parameters and titanium contents, and produced the first TiO_2 abundance map of the entire Moon. This analysis further verified that Mare Tranquillitatis was indeed the most titanium-rich mare on the Moon (Plate 3 in Lucey et al., 1998), although their algorithms may produce greater errors at high titanium contents. Reconstruction of the titanium content map using Clementine data and the equations of Lucey et al. (2000) shows that extensive areas of the mare surface surrounding craters Ross and Maclear in northwestern Mare Tranquillitatis have extremely high TiO_2 contents of up to ~18 wt.% (Figure S1). These estimated TiO_2 content values exceed the compositional range of returned basalt samples and basaltic lunar meteorites (McKay et al., 1991; Korotev & Irving, 2021) and are likely of greater inaccuracy due to the limitation of the algorithm and artifacts in the Clementine global data sets (e.g., imperfect mosaicking and photometric calibration). Sato et al. (2017) collected over five years of repeat reflectance measurements of sample-return sites acquired by LROC WAC and found a linear correlation between TiO_2 contents and the 321/415 nm band ratio, from which a new near-global TiO_2 abundance map was constructed. This new titanium map is more consistent with compositions of lunar basalt samples and Lunar Prospector Gamma-Ray Spectrometer titanium measurement (generally within ±0.3 wt. % for Tranquillitatis basalts). This new map shows clearly that the northwestern portion of Mare Tranquillitatis indeed has the highest TiO_2 content on the entire Moon, with a refined value of ∼12.6 wt. % (Figure 1C).

The basalt deposits of Mare Tranquillitatis are also characterized by significant compositional variation (Figure 1C) and the stratigraphic relationships reveal the complicated and multi-phase volcanic infilling events. First examinations of Apollo 11 samples recognized two groups of high-Ti mare basalts (types A and B; LSPET, 1969): Group A is high-K basalt and dated to be 3.57 Ga; Group B is low-K basalts and dated at 3.66-3.85 Ga (Wilhelms, 1987 and references therein). Subsequent detailed characterizations divided Group B samples into three sub-groups (B1, B2 and B3; Beaty & Albee, 1978) and identified an additional group (Group D, also low-K but more REE-enriched; Beaty et al., 1979). Integrating chronological and geochemical measurements suggested three major volcanic eruptions at the Apollo 11 site: the earliest eruption occurred at ~3.85 Ga and emplaced basalts represented by Group B2 and D basalts (8.4–8.9 wt. % TiO_2); subsequent activity produced the B1 and B3 basalts (~10.2 wt. % TiO_2) at 3.69–3.75 Ga, and the final phase of eruption took place at 3.58 Ga and produced Group A basalts (11.0 wt. % TiO_2) (Jerde et al., 1994; Snape et al., 2019). This context is important as a baseline in interpreting the formation of mare domes and their relation to the infilling history of Mare Tranquillitatis.

Analyses of remote sensing imaging and spectral data enable the characterization of the stratigraphy and chronology of the entire Mare Tranquillitatis beyond the very local surface area represented by the Apollo 11 samples. During the 1960s and 1970s, the lunar nearside was geologically mapped in 44 quadrangles using mainly Lunar Orbiter imager data (each quadrangle covers an area of 20°×16°). In these maps, the basalt deposits of Mare Tranquillitatis were mainly interpreted as Imbrian-aged mare flows, with multiple infilling sequences (Im1-3 or Ipm1-4; Carr, 1966; Morris & Wilhelms, 1967; Milton, 1968; Elston, 1972; Wilhelms, 1972; Scott & Pohn, 1972). In addition, some possible Eratosthenian mare units (Em) were identified in the northeast (Scott & Pohn, 1972) and along the southeastern margin (Wilhelms, 1972). Boyce (1976) divided Mare Tranquillitatis into four units on Lunar Orbiter photographs and estimated two ages (3.6 ± 0.1 and 3.75 ± 0.05 Ga) from crater degradation studies. On the basis of spectral parameters derived from telescope spectroscopic measurements, Pieters (1978) subdivided the Mare Tranquillitatis basalts into three major spectral units (HDWA, mIG-, and "undivided" units). Staid et al. (1996) analyzed the Galileo multi-spectral data of Mare Tranquillitatis and divided the mare basalt fill into four distinct mare types, and found that the younger mare units were generally more titanium-rich than the older maria.

The development of the planetary surface dating method using crater statistics enabled the determination of the absolute ages of abundant lunar mare units (despite many existing challenges). Hiesinger et al. (2000) identified 27 stratigraphic units in Mare Tranquillitatis from

Galileo spectral data and dated these units to be 3.39–3.80 Ga from crater population measurements on Lunar Orbiter IV images (60-150 m/pixel), which placed the entire Mare Tranquillitatis basalts in the Imbrian system (Figure 1D). Putting these ages in the context of the global lunar maria dated subsequently showed unequivocally that Mare Tranquillitatis is the oldest major mare on the Moon (Figure 2A and references in the caption). We investigated the age variations of basalt units identified in 19 out of 23 maria on the entire Moon (Andersson & Whitaker, 1982; the other four maria, Anguis, Spumans, Undarum and Nectaris, are not dated) and plot them in quartile values (Figure 2B). All but one of the basalt units in Mare Tranquillitatis are older than 3.5 Ga, with a median value of ~3.7 Ga. Only Mare Humboldtianum basalts are of ages similar to Mare Tranquillitatis (3.4–3.84 Ga, median value of ~3.7 Ga). However, Mare Humboldtianum basalts occur as several small and sporadic mare ponds, and the mare is nearly one order of magnitude smaller (total surface area 5.45×10^4 km^2) than the extensive (3.97×10^5 km^2) and continuous Mare Tranquillitatis basalt deposits. In summary, mare deposits in Mare Tranquillitatis represent the earliest major phase of exposed mare volcanism, and investigation of their detailed characteristics should provide fundamental insights into the early geologic and thermal evolution of the Moon.

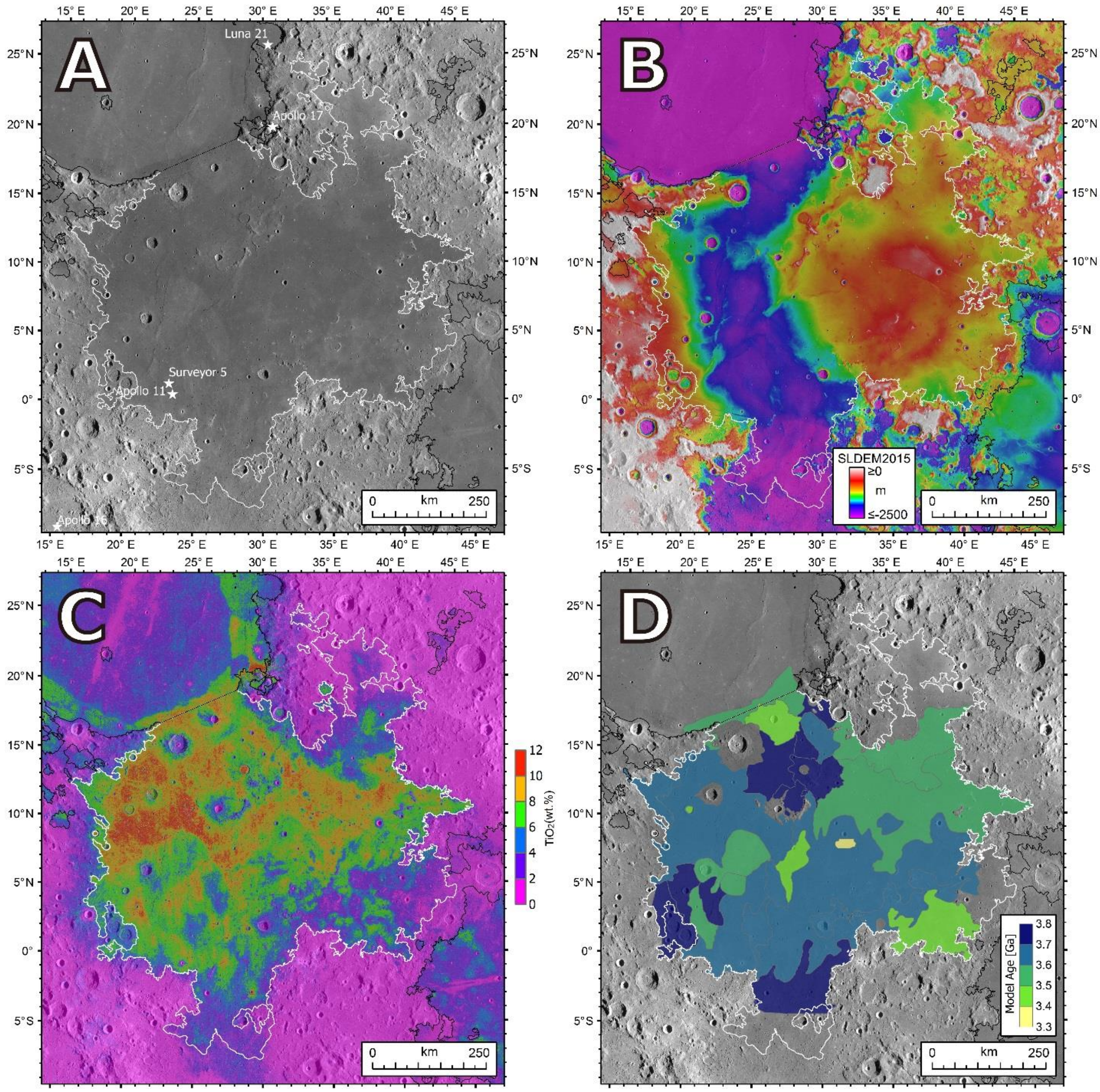

Figure 1. Maps of Mare Tranquillitatis: (A) LROC WAC low-Sun mosaic (100 m/pixel), (B) colorized SLDEM2015 topography (512 pixels per degree), (C) TiO_2 content calculated from LROC WAC multi-band reflectance image (Sato et al., 2017), and (D) absolute model age of mare units derived from the crater population method (Hiesinger et al., 2000). The landing locations of several landed missions (Apollo 11 and 17, Luna 21 and Surveyor 7) are labeled in panel A. The outline of Mare Tranquillitatis and adjacent maria (Nelson et al., 2014) are delineated by white and black lines, respectively. All the maps for the Mare Tranquillitatis region in this paper are projected into a Lambert conformal conic projection with a central meridian of 30° and two standard parallels of 2° and 16°, and north is up.

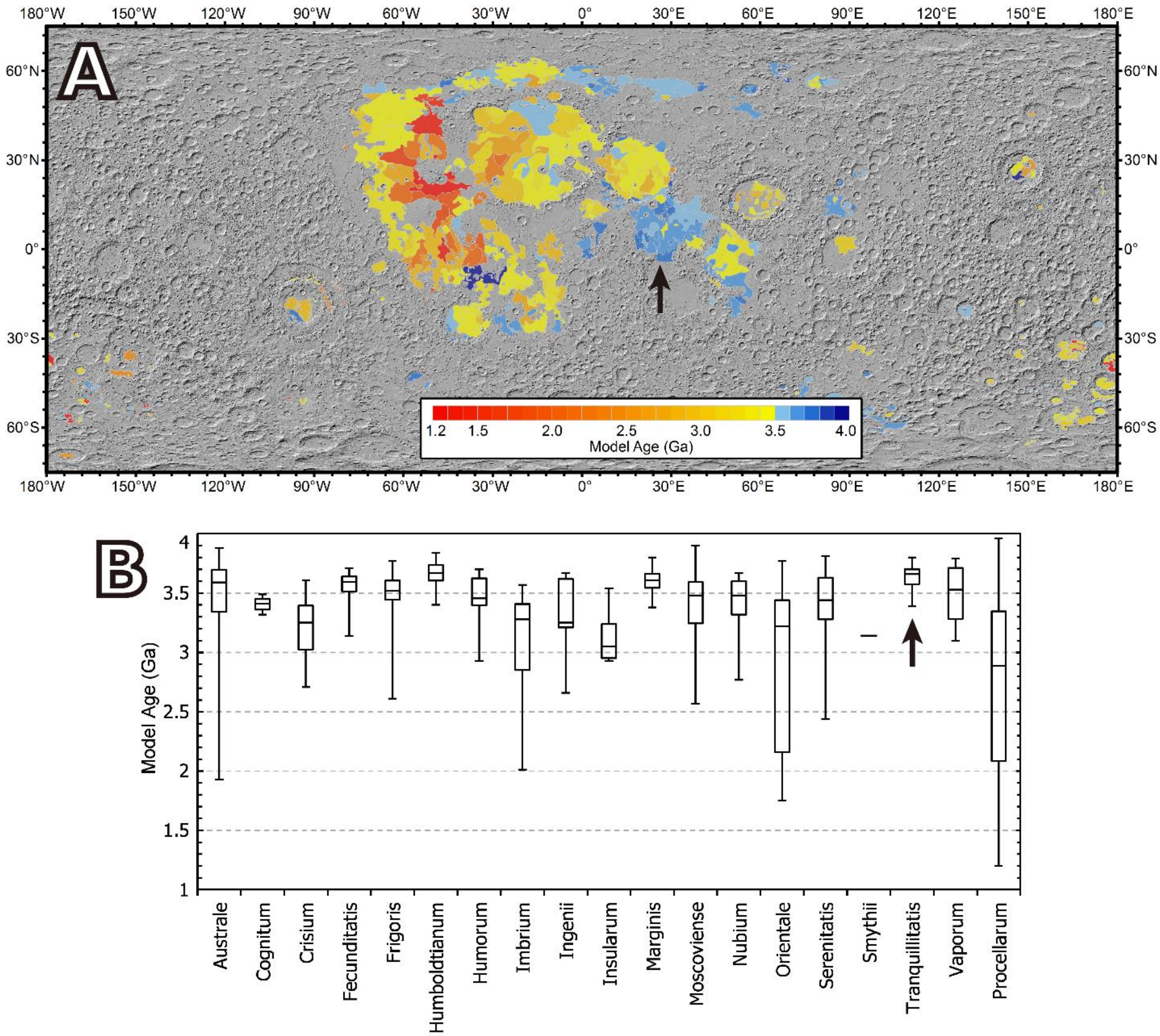

Figure 2. (A) Global map of model ages of mare basalts units (n = 482) estimated from crater population measurements (Cho et al., 2012; Haruyama et al., 2009; Hiesinger et al., 2006; Hiesinger, Head, et al., 2011; Hiesinger, van der Bogert, et al., 2011; Morota et al., 2009, 2011; Pasckert et al., 2015, 2018; Tyrie, 1998; Whitten et al., 2011). The basemap is a hillshade rendering (315° azimuth and 45° altitude) of LOLA 128 pixel/degree topography. (B) The minimum, first quartile, median, third quartile, and maximum age of mare units in each maria are shown. Mare Tranquillitatis is pointed out by black arrows in both panels.

4. Mare Dome Identification in Mare Tranquillitatis

We conducted a preliminary survey of previously catalogued mare domes (Head & Gifford, 1980; Wöhler et al., 2006, 2007; Tye & Head, 2013) using the latest high-precision and high-resolution altimetric and imaging data sets (Section 2), and defined some fundamental characteristics of mare domes. A typical well-developed mare dome is characterized by a domical raised structure with a generally convex-upward shape and low-slope (<5°) profile, and a (quasi-)circular or elliptical outline. Some domes have summit pit craters, while many lack them, possibly being filled up by the last extruded lavas. The development of the circular mound shape of mare domes is sometimes influenced by pre-existing topography; in these cases, the outline of the dome on the side near the pre-existing topography will be poorly defined, while at the side distal to the pre-existing topography, the circular mound shape will be relatively well developed, forming an arc-shaped shield base outline. On the basis of these observations and documentation, we first evaluated each mare dome identification in previous investigations and then searched for new mare dome features in Mare Tranquillitatis. The recognition of these typical characteristics of mare domes, including the (quasi-)circular or elliptical map-view outline and domical raised structure, help confirm a mare dome identification (definite domes). The lack of parts of, or the irregularity of these dome characteristics, such as domes occurring in sloped or complex terrains, decreases the dome identification reliability (possible domes). Summit pit features are not the key criteria for dome identification, as many mare domes lack summit pits (e.g., Head & Gifford, 1980), although their presence enhances the identification reliability of the subjacent mare dome. The absence of most of these dome characteristics would prevent the confident identification of a dome feature (questionable domes).

4.1 Evaluations of Previous Mare Dome Identifications in Mare Tranquillitatis

There are three prior dedicated mare dome identification contributions in Mare Tranquillitatis (Table S1), and each is re-evaluated as follows:

(1) Head and Gifford (1980) identified 36 mare domes in Mare Tranquillitatis, informally named as Cauchy 1-5, Sina 1-3, Jansen 1-8, Arago 1-6, Maskelyne 1 and Vitruvius 1-13, using telescopic (Consolidated Lunar Atlas) and orbital photographs (Apollo) obtained under variable illumination conditions (especially low-Sun illumination). Of these catalogued domes, all but one (Cauchy 3) are re-confirmed in our new data-based investigations (Figure 3). The majority of these domes are found in northern Mare Tranquillitatis, and this observational discrepancy (compared with the abundant domes identified in later studies in the south) is probably due to the coverage and illumination condition variations of the images employed.

(2) Tye and Head (2013) identified 67 additional (other than those in Head and Gifford (1980)) domes in Mare Tranquillitatis using LOLA topography data (another 12 additional domes occur in Mare Fecunditatis and Crisium). Of their reported additional Tranquillitatis domes, 54 domes are re-confirmed on our new data sets, five are relatively poorly defined and eight are of questionable existence (Figure 3). Over half of these domes (n = 35) occur on the large broad rise in eastern Mare Tranquillitatis (Figure 1B), elevated up to 2.2 km above the surrounding maria (Tye & Head, 2013).

(3) Wöhler, Lena, and their colleagues conducted a series of independent identifications of lunar mare domes using their own Earth-based telescopic images (Wöhler et al., 2006, 2007,

2009). Among their 28 detected mare domes (termed as A1-7, C1-13, Ca1, D and NTA1-6) in Mare Tranquillitatis, 16 were previously documented in Head and Gifford (1980), another five were catalogued in Tye and Head (2013), and the remaining seven domes are new identifications not listed elsewhere. Of the seven new domes, four are re-confirmed in our investigations, two are poorly defined, and one is of questionable existence (Figure 3).

Note that in some very early telescope-based mare dome identification reports (e.g., Jamieson, 1965; Rae, 1966; Smith, 1973), the dome locations were usually not reported in lunar latitude and longitude, but in coordinates relative to the photo frames margins and other forms. These locations have great uncertainties and relocating these domes is very challenging and these dome identifications were not re-assessed here.

4.2 New Mare Domes Identified in Mare Tranquillitatis

Using new SLDEM2015 topography and other new data sets for Mare Tranquillitatis described above, we conducted a systematic search for mare dome features in this region. We identified 96 new domes in Mare Tranquillitatis (Figure 3), which brings the total number of confirmed domes in this region to 189. We also find evidence for another 87 possible mare domes, in addition to seven possible domes catalogued previously (Section 4.1 and Figure 3). These observations show that Mare Tranquillitatis contains one of the highest densities of mare domes among the entire lunar maria (Head & Gifford, 1980). Crater count dating has shown that Mare Tranquillitatis is the oldest major mare on the Moon, with ~90% of mare units emplaced between 3.5 and 3.8 Ga ago (Hiesinger et al., 2000), indicating that shield-building eruptions may be a prevalent volcanic eruption style in the earliest stage of lunar volcanism, providing a potentially important constraint into the relation of mare volcanism and lunar thermal evolution history (e.g., Head & Wilson, 2017).

By using the locations of the 283 domes (189 definite and 94 possible), we calculated their areal density in a moving neighbor circle of 50 km in radius (Figure S2). The density map shows clearly that the spatial distribution of mare domes in Mare Tranquillitatis is highly inhomogeneous. Two regions of significant concentration of mare domes are observed. One is at the northern mare margin and east of Jansen crater (Figures 3 and S2), which occurs as a broad arc-shaped area, with a size of ~300 × 150 km. This area was shown previously to be populated by many mare domes (e.g., Head & Gifford, 1980), while our updated survey expands significantly the number of domes by four times to over 90. Another prominent region of dome concentration is in the southern part of Mare Tranquillitatis, between craters Maskelyne and Sinas (Figures 3 and S2), which was recognized previously as a broad rise (Tye & Head, 2013). In this local area, ~300 × 200 km in size, 133 mare domes are identified, nearly 50% more domes than in the northern area. Most of our newly-identified mare domes (103/183) also occur in this southern area. In addition, two smaller areas (diameter <100 km), one north of crater

Arago and another west of Carrell crater, also show regional concentration of nearly ten dome features (Figures 3 and S2).

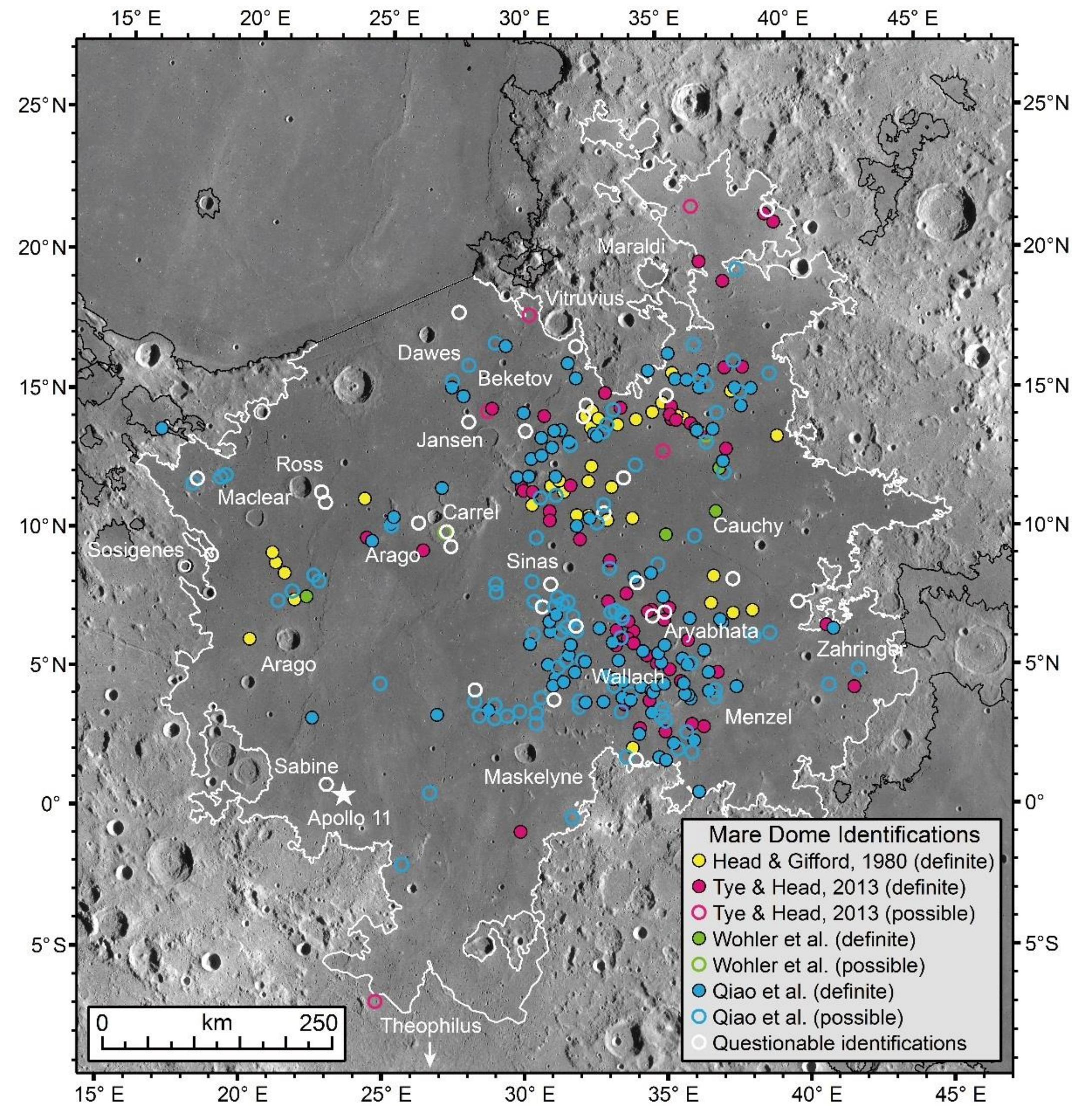

Figure 3. Spatial distribution of mare domes in Mare Tranquillitatis identified by prior studies (Table S1) and this analysis (Table 1). Confirmed domes are marked with solid circles, possible domes are marked with colored open circles, and questionable dome identifications are white circles. Names of prominent impact craters used for dome nomenclature are labelled.

4.3 Nomenclature

Hundreds of domes have been discovered in Mare Tranquillitatis in this study (Figure 3). To facilitate communications, we propose an informal nomenclature for these domes. First, dome names previously designated by Head and Gifford (1980) are adopted (Table S1). Other unnamed dome features identified (including both definite and possible identifications) in the vicinity of a significant IAU-named crater (the “parent” or “patronymic” crater) are designated by the name of the crater and a numeral. The numbering starts from the dome or dome cluster at the north point and then proceeds clockwise, similar to the scheme for letter-designed craters on the Moon (Andersson & Whitaker, 1982). Questionable dome identifications are also similarly numbered (Table 1).

Table 1. List of Catalogued Mare Domes in Mare Tranquillitatis and Their Characteristics.

	Mare Dome										Summit Pit Crater					
Name	Lat [°]	Long [°]	Reliability[1]	Shape[2]	Diameter (km)	Ellipticity	Height (m)	Volume (km^3)	Mean slope [°]	Host mare age [Ga]	Reliability[1]	Shape[2]	Diameter (km)	Ellipticity	Depth (m)	Volume (km^3)
Arago 1	6.14	20.03	A	I	12.4	1.22	305.5	21.08	3.3	3.7	C	–	–	–	–	–
Arago 2	7.55	21.56	A	I	21.0	1.29	397.9	44.42	3.5	3.7	B	E	0.8	1.91	23.4	0.00235
Arago 3	8.53	21.20	A	C~	12.6	1.12	122.9	8.86	2.3	3.7	A	E~	0.8	1.38	28.5	0.00390
Arago 4	8.93	20.89	A	C~	9.1	1.10	81.1	3.03	2.3	3.7	A	G	1.6	2.48	27.6	0.00792
Arago 5	9.27	20.76	A	E~	7.2	1.44	113.1	2.54	2.6	3.7	A	G	1.9	2.38	145.2	0.10533
Arago 6	11.28	24.12	A	C~	5.6	1.16	103.1	1.17	3.2	3.7	A	E~	0.9	1.64	36.8	0.00878
Arago 7	7.55	21.00	B	E~	5.2	2.14	103.8	1.11	3.0	3.7	A	I	0.9	1.43	18.9	0.00164
Arago 8	7.91	21.53	B	E~	4.6	1.53	83.5	0.79	2.6	3.7	A	C~	0.7	1.29	27.2	0.00313
Arago 9	7.71	22.05	A	C~	3.7	1.16	93.1	0.41	3.4	3.7	A	E~	0.9	1.52	49.3	0.00645
Arago 10	8.48	22.29	B	E	5.3	2.40	81.1	0.87	2.9	3.7	B	E	0.7	1.43	37.0	0.00510
Arago 11	8.31	22.50	B	E	11.6	2.66	123.8	6.27	2.6	3.7	B	E~	0.6	1.22	22.9	0.00225
Arago 12	4.62	24.77	B	E~	10.6	1.63	133.5	6.09	2.8	3.6	A	C	1.2	1.07	149.6	0.05773
Arago 13	3.35	22.34	A	I	10.4	1.16	118.7	4.46	2.3	3.7	B	C	0.5	1.13	48.9	0.00279
Aryabhata 1	7.23	34.48	A	E	4.8	1.31	38.4	0.29	2.3	3.6	C	–	–	–	–	–
Aryabhata 2	7.28	34.61	A	E~	3.7	1.26	36.6	0.17	2.1	3.6	C	–	–	–	–	–
Aryabhata 3	6.90	35.06	A	E~	8.0	1.35	46.8	0.74	2.4	3.6	A	E	0.7	1.72	23.4	0.00307
Aryabhata 4	7.35	35.24	A	I	3.9	1.12	53.9	0.26	2.8	3.6	A	E~	0.6	1.24	32.9	0.00324
Aryabhata 5	7.75	35.06	A	C~	2.9	1.09	49.1	0.09	2.4	3.6	C	–	–	–	–	–
Aryabhata 6	8.46	34.01	A	E	5.9	1.33	43.2	0.48	2.4	3.6	B	I	0.7	1.98	16.3	0.00145
Aryabhata 7	8.61	34.62	A	E~	4.6	1.33	45.6	0.24	2.2	3.6	A	G	1.0	4.47	23.0	0.00374
Aryabhata 8	9.02	34.92	B	I	16.6	1.49	57.7	4.02	2.3	3.6	A	E~	0.8	1.32	73.0	0.01471
Aryabhata 9	6.97	36.02	A	C~	5.3	1.12	37.6	0.30	2.0	3.6	B	G	0.6	2.75	16.6	0.00171
Aryabhata 10	6.20	35.95	A	I	11.5	1.37	155.0	8.64	2.6	3.6	A	G	0.7	2.52	26.0	0.00288
Aryabhata 11	5.80	36.53	A	I	10.0	1.45	192.0	6.98	3.1	3.6	C	–	–	–	–	–
Aryabhata 12	5.50	35.73	A	C	3.4	1.10	51.2	0.18	2.8	3.6	A	E	0.9	1.33	70.2	0.01453
Aryabhata 13	5.28	35.92	A	I	3.9	1.55	51.7	0.29	2.4	3.6	A	I	0.7	1.43	51.0	0.00483

	Mare Dome										Summit Pit Crater					
Name	Lat [°]	Long [°]	Reliability[1]	Shape[2]	Diameter (km)	Ellipticity	Height (m)	Volume (km^3)	Mean slope [°]	Host mare age [Ga]	Reliability[1]	Shape[2]	Diameter (km)	Ellipticity	Depth (m)	Volume (km^3)
Aryabhata 14	5.39	36.08	B	C~	7.5	1.13	67.9	1.45	2.6	3.6	B	C	0.9	1.02	108.1	0.02338
Aryabhata 15	6.01	35.12	A	C~	8.8	1.12	83.7	2.02	2.8	3.6	A	E~	1.8	2.09	115.5	0.11553
Aryabhata 16	5.12	35.25	A	C~	6.5	1.09	112.6	1.46	3.0	3.6	A	I	0.7	1.17	13.5	0.00108
Aryabhata 17	5.38	34.95	A	E~	2.8	1.56	39.2	0.09	2.6	3.6	A	E	0.8	1.42	53.7	0.01119
Aryabhata 18	5.36	34.79	A	E~	4.3	1.36	82.7	0.48	2.7	3.6	A	G	1.0	2.56	12.7	–
Aryabhata 19	5.78	34.88	A	E~	11.3	1.85	103.4	3.28	2.3	3.6	A	C~	0.4	1.25	17.6	0.00046
Aryabhata 20	5.65	34.46	A	I	5.0	1.44	43.7	0.36	2.4	3.6	B	G	0.4	13.94	12.5	–
Aryabhata 21	5.80	34.31	A	E~	2.8	1.28	26.0	0.07	2.3	3.6	B	C	0.3	1.14	25.5	0.00080
Aryabhata 22	6.05	33.93	A	C~	5.9	1.06	57.5	0.80	2.5	3.6	C	–	–	–	–	–
Aryabhata 23	6.26	33.76	A	E~	5.4	1.27	66.2	0.67	2.4	3.6	A	I	0.7	1.55	32.7	0.00351
Aryabhata 24	6.28	33.50	B	C~	2.9	1.17	47.2	0.14	2.4	3.6	B	C	0.3	1.14	14.3	0.00031
Aryabhata 25	6.12	33.20	A	E	2.0	1.25	71.0	0.08	4.3	3.6	B	C	0.4	1.06	3.8	–
Aryabhata 26	6.02	33.33	A	C~	4.2	1.14	38.0	0.23	2.1	3.6	C	–	–	–	–	–
Aryabhata 27	6.50	33.97	A	C	10.6	1.06	104.9	3.06	2.5	3.6	A	E	1.1	1.78	78.6	0.02502
Aryabhata 28	6.58	33.34	A	C~	5.5	1.18	53.8	0.41	2.4	3.6	C	–	–	–	–	–
Aryabhata 29	6.64	32.72	A	E	2.8	1.23	56.0	0.14	3.4	3.6	A	E~	1.2	1.76	78.1	0.03936
Aryabhata 30	6.87	33.76	A	E	3.4	1.17	69.5	0.23	3.1	3.6	A	I	0.9	1.76	43.1	0.00677
Aryabhata 31	7.01	33.56	B	I	6.3	1.30	48.4	0.37	2.5	3.6	B	G	0.8	2.22	23.4	0.00363
Aryabhata 32	7.14	33.56	B	I	4.4	1.24	62.6	0.35	2.7	3.6	A	C~	1.1	1.13	129.6	0.04894
Aryabhata 33	7.27	33.33	B	I	3.7	1.35	25.4	0.08	2.3	3.6	A	E	0.5	1.63	31.9	0.00151
Aryabhata 34	7.23	33.14	B	I	9.3	1.32	36.3	0.84	2.0	3.6	C	–	–	–	–	–
Aryabhata 35	7.57	33.00	A	E~	10.6	1.23	61.3	2.33	2.4	3.6	C	–	–	–	–	–
Aryabhata 36	7.89	33.70	A	E~	5.1	1.17	80.0	0.58	2.8	3.6	A	G	0.5	2.92	16.1	0.00064
Beketov 1	16.82	29.29	A	I	11.1	1.21	111.0	5.68	3.1	3.7	C	–	–	–	–	–
Beketov 2	16.88	28.89	B	I	8.8	1.35	104.2	3.50	2.6	3.7	C	–	–	–	–	–
Carrel 1	11.74	26.93	A	E~	6.0	1.58	46.6	0.49	2.5	3.7	A	E~	0.9	1.38	99.4	0.02512
Carrel 2	10.11	27.08	B	I	2.6	1.03	67.4	0.14	3.6	3.7	C	–	–	–	–	–

	Mare Dome										Summit Pit Crater					
Name	Lat [°]	Long [°]	Reliability[1]	Shape[2]	Diameter (km)	Ellipticity	Height (m)	Volume (km^3)	Mean slope [°]	Host mare age [Ga]	Reliability[1]	Shape[2]	Diameter (km)	Ellipticity	Depth (m)	Volume (km^3)
Carrel 3	9.44	26.31	A	I	6.1	1.16	56.2	0.83	2.1	3.7	A	I	0.7	1.51	21.9	0.00234
Carrel 4	10.32	25.12	B	I	2.6	1.55	71.1	0.14	3.3	3.7	B	C	0.8	1.09	96.5	0.01808
Carrel 5	10.39	25.08	A	E~	3.7	1.39	80.0	0.34	3.1	3.7	C	–	–	–	–	–
Carrel 6	10.64	25.20	A	I	3.5	1.31	40.2	0.16	2.4	3.7	C	–	–	–	–	–
Carrel 7	9.77	24.43	A	I	5.2	1.66	82.7	0.86	3.0	3.7	B	C	0.6	1.12	75.4	0.00666
Carrel 8	9.88	24.25	A	E	8.1	1.90	144.7	3.61	3.0	3.7	A	E~	2.4	1.71	322.9	0.53307
Cauchy 1	7.22	38.31	A	C	8.9	1.04	122.5	4.80	2.9	3.6	A	E	1.6	1.22	209.1	0.17737
Cauchy 2	7.52	36.76	A	C	9.9	1.19	249.2	8.44	3.9	3.6	C	–	–	–	–	–
Cauchy 4	8.50	36.93	A	E	9.2	1.13	70.8	2.07	2.3	3.6	A	E	1.7	1.76	108.8	0.11674
Cauchy 5	7.14	37.60	A	C	5.7	1.14	56.3	0.49	2.9	3.6	A	E	1.8	2.63	63.7	0.05545
Cauchy 6	6.90	37.12	A	C~	1.8	1.09	76.5	0.07	4.8	3.6	C	–	–	–	–	–
Cauchy 7	6.78	37.20	A	E	3.1	1.24	73.7	0.25	3.6	3.6	B	C~	0.4	1.16	11.5	0.00054
Cauchy 8	6.28	38.37	B	E~	4.6	1.72	56.6	0.40	2.4	3.6	B	C	0.9	1.18	47.8	0.00919
Cauchy 9	6.39	38.94	B	I	3.1	1.34	38.2	0.08	2.3	3.6	B	C~	0.4	1.09	18.4	0.00065
Cauchy 10	10.00	35.19	A	C~	5.2	1.19	70.8	0.70	2.6	3.6	A	E	1.5	1.44	168.6	0.10405
Cauchy 11	9.96	36.25	B	I	15.3	1.38	58.2	3.08	2.6	3.6	B	E	0.5	1.07	23.6	0.00120
Cauchy 12	10.86	37.02	A	I	20.9	1.40	125.6	23.24	2.7	3.6	B	C~	0.5	1.18	47.0	0.00373
Jansen 1	11.55	31.44	A	I	12.1	1.23	168.5	4.95	2.7	3.6	C	–	–	–	–	–
Jansen 2	11.11	30.28	A	E	6.3	1.53	85.2	0.88	2.7	3.6	B	C	0.4	1.10	14.2	0.00064
Jansen 3	11.77	30.98	A	C~	4.3	1.11	80.2	0.35	2.5	3.6	C	–	–	–	–	–
Jansen 4	11.96	31.27	A	C~	4.8	1.09	73.1	0.44	2.7	3.6	A	E	0.8	1.37	70.7	0.01670
Jansen 5	12.48	32.46	A	C~	6.1	1.14	63.6	0.82	2.3	3.6	C	–	–	–	–	–
Jansen 6	11.94	32.35	A	E~	14.1	1.25	119.8	8.11	2.7	3.6	A	E	3.3	1.49	625.8	1.91094
Jansen 7	11.76	33.21	A	E	11.5	1.21	53.5	1.96	2.3	3.6	A	G	2.4	3.95	162.2	0.27897
Jansen 8	10.62	33.97	A	E	6.7	1.15	74.3	0.95	2.6	3.6	A	C	0.5	1.15	34.5	0.00324
Jansen 9	14.47	28.67	B	I	3.9	1.27	106.0	0.36	3.5	3.8	A	G~	2.1	2.19	83.6	0.05201
Jansen 10	14.57	28.77	A	I	4.6	1.10	89.6	0.81	2.6	3.8	A	E	0.7	1.23	49.9	0.00695
Jansen 11	14.43	29.97	A	E	3.0	1.34	71.0	0.25	3.4	3.7	C	–	–	–	–	–

	Mare Dome										Summit Pit Crater					
Name	Lat [°]	Long [°]	Reliability[1]	Shape[2]	Diameter (km)	Ellipticity	Height (m)	Volume (km^3)	Mean slope [°]	Host mare age [Ga]	Reliability[1]	Shape[2]	Diameter (km)	Ellipticity	Depth (m)	Volume (km^3)
Jansen 12	14.34	30.75	A	E	10.3	1.33	374.1	17.23	5.0	3.8	A	I	0.9	1.15	37.2	0.00593
Jansen 13	13.53	30.62	A	E~	5.5	1.24	124.7	1.70	3.1	3.8	B	C	0.6	1.06	43.0	0.00305
Jansen 14	13.77	31.11	A	C~	4.0	1.18	55.9	0.21	2.4	3.8	B	C	0.4	1.20	9.5	0.00037
Jansen 15	13.79	31.33	A	I	5.3	1.35	78.2	0.94	2.7	3.8	A	C~	0.9	1.15	71.3	0.01640
Jansen 16	13.39	31.65	A	C~	5.0	1.15	49.2	0.27	2.6	3.6	A	G	1.4	2.39	101.4	0.04161
Jansen 17	13.25	31.69	B	I	5.2	1.21	24.7	0.18	2.1	3.6	B	C	0.6	1.14	41.8	0.00509
Jansen 18	13.17	31.01	A	I	6.1	1.19	167.5	3.15	3.5	3.8	B	E~	0.8	1.17	29.7	0.00535
Jansen 19	12.96	30.64	A	I	20.0	1.35	252.9	37.42	3.0	3.8	B	E~	1.2	1.22	86.8	0.03788
Jansen 20	12.77	30.26	A	E	3.1	1.46	86.6	0.27	3.6	3.8	B	E~	0.5	1.22	10.4	0.00010
Jansen 21	12.13	30.16	A	C~	4.2	1.08	81.9	0.45	3.3	3.8	B	I	0.5	1.20	12.3	0.00080
Jansen 22	12.09	29.74	A	E	4.0	1.61	148.6	0.91	5.2	3.8	B	E	0.5	1.28	18.3	0.00120
Jansen 23	11.74	29.91	A	I	5.5	1.13	61.7	0.52	2.8	3.8	C	–	–	–	–	–
Jansen 24	11.62	29.97	A	C~	2.1	1.16	36.3	0.06	2.7	3.8	C	–	–	–	–	–
Jansen 25	11.57	30.27	A	C~	3.6	1.14	84.0	0.40	3.3	3.6	A	E	0.4	1.76	8.3	0.00008
Jansen 26	11.36	30.58	B	E~	2.1	1.20	40.5	0.05	3.1	3.6	B	E~	0.5	1.73	17.8	0.00036
Jansen 27	11.41	31.16	B	E~	6.3	1.49	27.8	0.36	2.0	3.6	C	–	–	–	–	–
Jansen 28	12.12	31.16	A	I	4.8	1.48	51.6	0.30	2.3	3.6	C	–	–	–	–	–
Jansen 29	11.78	31.72	A	C~	8.4	1.11	58.9	1.42	2.2	3.6	C	–	–	–	–	–
Jansen 30	12.53	34.09	B	I	5.7	1.53	30.0	0.13	2.1	3.6	C	–	–	–	–	–
Jansen 31	15.02	27.75	A	C~	5.2	1.05	47.5	0.40	2.3	3.7	B	E	0.4	1.58	16.3	0.00081
Jansen 32	15.33	27.31	A	I	7.1	1.09	120.3	1.59	3.3	3.7	A	C	0.9	1.08	71.3	0.01899
Jansen 33	15.55	27.31	B	I	5.5	1.28	59.4	0.66	2.5	3.7	A	G	1.2	2.65	15.6	0.00223
Jansen 34	16.13	27.92	B	E	3.3	1.34	46.3	0.14	2.9	3.7	A	C	0.7	1.08	31.4	0.00449
Maclear 1	11.93	18.78	B	E	4.2	1.18	59.6	0.28	2.7	3.7	B	G	0.8	2.24	27.7	0.00411
Maclear 2	12.06	18.99	B	I	5.1	1.14	35.7	0.23	2.6	3.7	B	C	0.5	1.20	15.8	0.00070
Maclear 3	11.71	17.75	B	I	5.0	1.36	122.3	0.99	3.7	3.6	A	C	1.6	1.04	182.8	0.12205
Maclear 4	13.64	16.57	A	C~	3.7	1.11	60.1	0.23	2.3	0	B	C~	0.6	1.10	23.2	0.00205
Maraldi 1	21.77	36.22	B	I	12.2	1.57	82.9	2.64	2.2	0	A	G	2.9	2.59	130.4	0.22606

	Mare Dome										Summit Pit Crater					
Name	Lat [°]	Long [°]	Reliability[1]	Shape[2]	Diameter (km)	Ellipticity	Height (m)	Volume (km^3)	Mean slope [°]	Host mare age [Ga]	Reliability[1]	Shape[2]	Diameter (km)	Ellipticity	Depth (m)	Volume (km^3)
Maraldi 2	19.79	36.55	A	E~	6.3	1.21	89.5	1.05	2.6	0	A	I	0.8	1.69	36.5	0.00496
Maraldi 3	19.49	37.98	B	E~	9.4	1.93	73.9	2.55	2.5	0	C	–	–	–	–	–
Maraldi 4	19.12	37.46	A	I	6.2	1.28	144.6	1.35	3.6	0	A	I	0.8	1.17	31.0	0.00372
Maraldi 5	21.45	39.07	A	I	6.9	1.23	123.5	1.17	3.4	0	A	I	2.1	1.50	78.7	0.09784
Maraldi 6	21.11	39.44	A	C	7.6	1.04	143.6	1.74	3.0	0	A	I	2.2	2.00	108.6	0.11002
Maskelyne 1	2.31	33.89	A	C	7.8	1.09	106.9	2.49	3.2	3.6	A	G	2.9	3.28	108.1	0.13705
Maskelyne 2	3.50	28.36	B	E~	7.7	1.95	81.4	1.73	2.6	3.6	C	–	–	–	–	–
Maskelyne 3	3.38	28.92	B	E~	8.6	2.05	83.3	2.27	2.4	3.6	C	–	–	–	–	–
Maskelyne 4	3.68	28.70	A	E~	5.4	1.27	47.4	0.43	2.4	3.6	C	–	–	–	–	–
Maskelyne 5	3.89	28.93	B	I	7.7	1.22	67.8	0.88	2.5	3.6	A	G	2.7	2.92	183.9	0.26180
Maskelyne 6	4.08	28.10	B	I	12.7	1.50	75.9	3.40	2.3	3.6	A	C~	0.7	1.11	40.1	0.00613
Maskelyne 7	3.48	29.38	B	I	6.7	1.14	44.6	0.60	2.4	3.6	C	–	–	–	–	–
Maskelyne 8	3.68	29.84	B	C~	9.2	1.17	47.4	1.31	2.1	3.6	C	–	–	–	–	–
Maskelyne 9	3.61	30.45	B	I	6.1	1.19	33.0	0.30	2.3	3.6	C	–	–	–	–	–
Maskelyne 10	3.27	30.46	B	I	17.6	1.20	77.4	8.17	2.5	3.6	B	E	0.7	1.31	31.5	0.00415
Maskelyne 11	3.05	34.14	A	I	11.9	1.16	120.8	4.58	2.6	3.6	C	–	–	–	–	–
Maskelyne 12	2.78	34.13	A	E~	8.6	1.51	114.9	3.86	2.3	3.6	B	G	1.2	2.33	32.0	0.00734
Maskelyne 13	2.00	33.65	B	I	19.3	1.25	333.8	18.31	2.7	3.6	B	G	1.0	1.98	28.0	0.00669
Maskelyne 14	-0.14	31.72	B	I	15.1	1.24	64.8	4.92	2.8	3.8	A	I	1.2	1.50	54.5	0.01924
Maskelyne 15	-0.66	29.71	A	I	22.8	1.11	244.0	48.92	2.9	3.8	A	I	1.3	1.52	47.7	0.01549
Maskelyne 16	-1.87	25.64	B	I	15.3	1.25	231.9	17.52	2.6	3.8	B	G	2.8	5.97	71.7	0.05588
Maskelyne 17	0.63	26.60	B	I	38.3	1.54	289.3	140.14	3.1	3.6	A	E	3.4	2.19	398.7	1.18823
Maskelyne 18	3.54	26.83	A	E~	11.7	1.27	89.4	3.09	2.4	3.6	A	G	1.7	2.08	44.2	0.02531
Menzel 1	4.12	36.88	B	I	4.1	1.22	34.4	0.18	2.1	3.6	B	E~	0.5	1.36	10.7	0.00057
Menzel 2	4.35	36.69	A	I	5.0	1.22	30.5	0.21	2.0	3.6	A	E~	0.5	1.40	14.2	0.00077
Menzel 3	4.32	36.91	B	I	5.5	1.52	30.1	0.19	2.2	3.6	B	C	0.8	1.10	41.1	0.00752
Menzel 4	4.47	37.67	A	C~	2.5	1.11	33.8	0.07	2.6	3.5	A	G	0.5	1.85	14.0	0.00057

	Mare Dome										Summit Pit Crater					
Name	Lat [°]	Long [°]	Reliability[1]	Shape[2]	Diameter (km)	Ellipticity	Height (m)	Volume (km^3)	Mean slope [°]	Host mare age [Ga]	Reliability[1]	Shape[2]	Diameter (km)	Ellipticity	Depth (m)	Volume (km^3)
Menzel 5	5.00	36.69	A	E~	8.1	1.39	36.1	0.52	2.1	3.6	C	–	–	–	–	–
Menzel 6	5.01	37.05	A	E~	13.8	1.26	69.9	3.38	2.3	3.6	C	–	–	–	–	–
Menzel 7	4.07	36.00	A	I	4.3	1.19	81.3	0.35	3.0	3.6	C	–	–	–	–	–
Menzel 8	4.18	35.92	A	E	4.3	1.38	64.1	0.40	2.6	3.6	B	E	0.6	1.29	20.9	0.00141
Menzel 9	4.22	35.81	A	E~	4.6	1.53	38.1	0.23	2.3	3.6	B	E	0.5	1.33	32.2	0.00192
Menzel 10	4.62	35.77	A	E~	2.9	1.30	74.4	0.20	3.1	3.6	C	–	–	–	–	–
Menzel 11	4.69	35.64	A	E~	6.2	1.23	59.8	0.71	2.6	3.6	A	I	0.7	2.11	40.2	0.00225
Menzel 12	4.60	35.06	A	E~	2.4	1.40	35.1	0.06	2.7	3.6	C	–	–	–	–	–
Menzel 13	4.56	34.76	A	I	6.9	1.14	79.2	0.84	3.2	3.6	A	E	1.2	1.38	55.2	0.01730
Menzel 14	4.37	34.59	A	E	3.4	1.22	76.4	0.22	3.1	3.6	A	I	0.7	1.45	33.1	0.00506
Menzel 15	4.31	34.65	A	C	2.1	1.11	51.8	0.06	4.2	3.6	C	–	–	–	–	–
Menzel 16	3.99	34.51	A	E	4.4	1.32	72.3	0.36	3.2	3.6	B	E~	0.7	1.35	19.3	–
Menzel 17	3.57	34.60	A	I	11.6	1.22	89.5	5.07	2.7	3.6	B	C	0.5	1.06	27.2	0.00215
Menzel 18	3.72	34.97	B	I	10.1	1.11	93.8	2.32	2.4	3.6	C	–	–	–	–	–
Menzel 19	3.42	34.95	B	E~	8.2	1.27	73.9	1.66	2.3	3.6	C	–	–	–	–	–
Menzel 20	3.27	35.09	B	I	6.5	1.49	62.2	0.67	2.6	3.5	A	E	0.6	1.19	25.0	0.00319
Menzel 21	2.94	35.15	A	E~	14.7	1.40	113.0	7.27	2.4	3.5	B	I	0.6	1.40	26.3	0.00287
Menzel 22	3.14	36.02	A	I	8.6	1.24	63.4	1.37	2.5	3.6	A	G	1.3	4.45	39.1	0.00792
Menzel 23	3.05	36.44	A	C~	4.4	1.12	53.0	0.31	2.5	3.6	B	E	0.4	1.41	11.5	0.00044
Menzel 24	2.84	35.83	B	I	9.9	1.39	58.8	1.68	2.3	3.5	C	–	–	–	–	–
Menzel 25	2.54	36.10	A	E~	11.6	1.20	58.7	2.05	2.6	3.5	B	C	0.5	1.13	21.5	0.00239
Menzel 26	2.13	35.99	B	E~	10.9	1.24	118.0	4.94	2.9	3.5	C	–	–	–	–	–
Menzel 27	2.27	35.50	B	I	4.1	1.50	27.7	0.12	2.5	3.5	B	E~	0.4	2.41	4.4	–
Menzel 28	2.46	35.37	A	E~	8.4	1.22	46.8	0.91	2.5	3.5	B	C~	0.4	1.27	18.3	0.00073
Menzel 29	1.91	35.08	A	C~	9.8	1.09	111.0	3.20	2.4	3.6	B	G	0.9	3.22	30.2	0.00233
Menzel 30	1.97	34.85	A	C~	3.9	1.14	104.1	0.45	3.5	3.6	C	–	–	–	–	–
Menzel 31	0.70	36.26	A	I	14.7	1.50	157.6	6.35	2.6	3.5	C	–	–	–	–	–

	Mare Dome										Summit Pit Crater					
Name	Lat [°]	Long [°]	Reliability[1]	Shape[2]	Diameter (km)	Ellipticity	Height (m)	Volume (km^3)	Mean slope [°]	Host mare age [Ga]	Reliability[1]	Shape[2]	Diameter (km)	Ellipticity	Depth (m)	Volume (km^3)
Sinas 1	10.53	33.05	A	C	8.1	1.07	99.8	2.79	2.9	3.6	A	C~	1.9	1.19	51.8	0.04354
Sinas 2	10.72	32.35	A	E~	4.3	1.27	111.4	0.65	3.3	3.6	A	E~	0.5	1.72	38.0	0.00325
Sinas 3	10.71	31.92	A	C	6.5	1.06	74.1	1.21	2.5	3.6	A	E	1.5	1.82	85.6	0.04518
Sinas 4	9.94	30.43	B	E~	7.4	1.74	71.6	1.57	2.2	3.6	C	–	–	–	–	–
Sinas 5	10.50	30.94	A	I	7.8	1.32	59.8	0.93	2.2	3.6	B	I	0.6	1.47	7.9	0.00039
Sinas 6	10.78	30.98	A	C~	12.6	1.19	97.7	6.30	2.4	3.6	A	E	1.1	1.91	57.4	0.02465
Sinas 7	9.86	32.08	A	I	2.7	1.61	42.9	0.10	2.8	3.6	C	–	–	–	–	–
Sinas 8	10.33	31.90	A	C~	5.8	1.08	40.3	0.31	2.4	3.6	A	C	0.8	1.12	63.3	0.01179
Sinas 9	10.61	32.40	A	I	5.0	1.25	62.9	0.57	2.7	3.6	C	–	–	–	–	–
Sinas 10	10.46	32.67	B	E~	3.9	1.29	29.2	0.15	2.0	3.6	B	C~	0.6	1.07	53.9	0.00515
Sinas 11	11.10	32.92	B	I	3.5	1.18	29.2	0.09	2.5	3.6	A	C~	0.8	1.06	59.4	0.01145
Sinas 12	9.06	33.11	A	C~	4.0	1.07	40.9	0.16	2.1	3.6	C	–	–	–	–	–
Sinas 13	8.81	33.12	B	I	4.0	1.28	28.0	0.10	2.5	3.6	B	C	0.3	1.09	9.6	0.00001
Sinas 14	7.60	31.59	B	C~	2.5	1.06	33.2	0.05	2.8	3.6	C	–	–	–	–	–
Sinas 15	7.53	31.40	B	I	9.3	1.43	63.6	1.61	2.4	3.6	B	C~	0.5	1.15	18.9	0.00092
Sinas 16	7.76	31.20	B	I	5.5	1.18	37.1	0.30	2.5	3.6	B	I	1.0	1.91	57.8	0.01351
Sinas 17	7.43	31.10	B	E~	4.9	1.36	26.3	0.12	2.3	3.6	B	E	0.5	1.60	16.5	0.00077
Sinas 18	7.14	31.14	A	C~	5.6	1.04	58.6	0.44	2.5	3.6	A	E	1.2	1.29	159.4	0.06896
Sinas 19	6.91	30.88	A	E~	4.2	1.58	67.6	0.22	3.0	3.6	A	C~	0.4	1.29	15.3	0.00086
Sinas 20	6.54	30.95	A	E	3.5	1.26	96.1	0.30	3.9	3.6	B	G	0.6	4.21	26.2	–
Sinas 21	6.50	31.32	B	I	3.7	1.16	22.0	0.07	2.0	3.6	A	C	0.7	1.11	40.3	0.00482
Sinas 22	6.69	31.52	B	I	4.2	1.19	34.6	0.14	2.1	3.6	C	–	–	–	–	–
Sinas 23	7.05	31.77	B	I	8.1	1.13	34.8	0.40	2.1	3.6	C	–	–	–	–	–
Sinas 24	6.55	31.88	B	I	5.0	1.24	21.3	0.10	2.3	3.6	A	E	0.5	1.33	21.6	0.00076
Sinas 25	6.40	30.33	B	E~	9.1	1.34	57.1	1.23	2.6	3.6	B	G	1.0	2.41	37.7	0.00863
Sinas 26	6.08	30.20	A	C	5.3	1.07	98.5	0.72	3.3	3.6	A	E	1.2	1.71	93.7	0.03297
Sinas 27	7.61	30.31	B	E~	8.4	1.48	41.9	0.80	2.2	3.6	B	C	0.6	1.17	66.9	0.00621

	Mare Dome										Summit Pit Crater					
Name	Lat [°]	Long [°]	Reliability[1]	Shape[2]	Diameter (km)	Ellipticity	Height (m)	Volume (km^3)	Mean slope [°]	Host mare age [Ga]	Reliability[1]	Shape[2]	Diameter (km)	Ellipticity	Depth (m)	Volume (km^3)
Sinas 28	8.31	30.26	B	I	8.5	1.87	51.8	1.00	2.4	3.6	C	–	–	–	–	–
Sinas 29	7.96	28.87	B	I	11.0	1.49	95.2	3.17	2.4	3.5	B	C~	0.7	1.23	38.2	0.00556
Sinas 30	8.25	28.94	B	I	5.3	1.12	47.6	0.37	2.2	3.6	C	–	–	–	–	–
Theophilus 1	-6.80	24.58	B	E~	86.9	1.35	540.7	1141.42	5.5	3.8	A	E~	3.8	1.45	328.6	1.36519
Vitruvius 1	14.21	35.88	A	C	6.7	1.07	140.9	2.81	3.4	3.6	A	I	1.3	1.44	71.1	0.04254
Vitruvius 2	14.29	35.65	A	E~	6.1	1.37	107.7	1.43	2.7	3.6	A	E~	1.4	1.57	168.2	0.09872
Vitruvius 3	14.76	35.10	A	C	9.2	1.12	81.0	2.09	2.5	3.6	C	–	–	–	–	–
Vitruvius 4	14.44	34.74	A	I	6.0	1.39	124.9	1.09	3.2	3.6	A	E	1.3	1.89	98.5	0.04914
Vitruvius 5	14.16	34.17	A	E~	10.1	1.24	64.5	2.33	2.1	3.6	A	G	2.2	2.82	199.2	0.28487
Vitruvius 6	14.00	33.47	A	C~	7.5	1.09	68.9	0.96	2.2	3.6	A	E~	0.6	1.46	38.1	0.00317
Vitruvius 7	14.30	32.29	A	C~	7.0	1.04	169.3	2.66	3.4	3.6	A	E	1.2	1.35	103.8	0.04433
Vitruvius 8	14.53	32.51	A	I	6.8	1.35	122.0	1.79	2.8	3.6	A	G	1.1	3.16	54.0	0.02517
Vitruvius 9	13.89	32.47	A	C~	5.0	1.10	91.2	0.78	2.8	3.6	B	C	0.7	1.04	55.3	0.00780
Vitruvius 10	14.23	32.76	A	E	11.3	1.45	107.8	3.73	2.5	3.6	A	E~	0.5	1.11	31.6	0.00265
Vitruvius 11	15.80	35.50	A	I	5.9	1.26	149.2	2.19	3.7	3.6	A	I	1.4	1.28	70.6	0.03664
Vitruvius 12	15.15	37.69	A	E	5.2	1.38	94.2	0.95	3.3	3.6	C	–	–	–	–	–
Vitruvius 13	13.43	39.38	A	C~	13.0	1.14	337.0	11.94	4.0	3.6	A	E	1.2	2.10	66.0	0.03052
Vitruvius 14	16.53	35.34	A	C~	2.5	1.15	78.5	0.15	3.8	3.6	C	–	–	–	–	–
Vitruvius 15	16.86	36.32	B	I	7.0	1.09	75.8	0.92	3.2	3.6	B	E~	0.8	1.67	58.7	0.00752
Vitruvius 16	15.93	34.61	A	C~	4.0	1.17	129.2	0.65	3.9	3.6	A	C	0.6	1.05	31.6	0.00326
Vitruvius 17	15.61	35.61	A	C~	4.5	1.09	85.8	0.45	3.2	3.6	B	I	0.5	1.57	16.0	0.00094
Vitruvius 18	15.59	36.03	A	E~	6.0	1.18	166.7	1.61	3.7	3.6	B	I	0.4	1.43	14.7	0.00069
Vitruvius 19	15.91	36.66	A	E	3.4	1.22	94.3	0.30	3.8	3.6	A	C	0.6	1.16	27.5	0.00182
Vitruvius 20	15.64	36.56	B	E~	5.7	1.50	42.6	0.53	2.3	3.6	C	–	–	–	–	–
Vitruvius 21	15.34	36.74	B	I	5.5	1.32	53.9	0.26	2.4	3.6	B	E~	0.7	1.68	30.7	0.00472
Vitruvius 22	15.26	36.49	A	I	10.0	1.19	41.0	1.09	2.3	3.6	A	E	0.7	1.59	62.3	0.01044
Vitruvius 23	15.97	37.49	A	C~	6.1	1.13	54.7	0.70	2.5	3.6	A	C~	0.9	1.05	61.5	0.01323
Vitruvius 24	16.22	37.81	B	E~	4.9	1.29	37.1	0.19	2.3	3.6	A	E~	0.3	2.09	9.6	0.00029

	Mare Dome										Summit Pit Crater					
Name	Lat [°]	Long [°]	Reliability[1]	Shape[2]	Diameter (km)	Ellipticity	Height (m)	Volume (km^3)	Mean slope [°]	Host mare age [Ga]	Reliability[1]	Shape[2]	Diameter (km)	Ellipticity	Depth (m)	Volume (km^3)
Vitruvius 25	15.99	38.12	A	C	3.6	1.10	149.7	0.71	5.9	3.6	A	C~	0.7	1.37	49.8	0.00691
Vitruvius 26	15.94	39.13	B	I	32.4	2.00	207.4	69.69	2.6	3.6	B	C	1.1	1.06	130.8	0.05031
Vitruvius 27	15.25	37.83	A	I	8.1	1.56	87.4	1.85	2.8	3.6	B	E~	0.9	1.64	62.3	0.01543
Vitruvius 28	15.10	38.03	B	I	7.7	1.37	35.2	0.47	2.5	3.6	A	E~	0.6	1.48	54.9	0.00521
Vitruvius 29	15.24	38.41	A	E~	7.4	1.41	35.0	0.44	2.5	3.6	C	–	–	–	–	–
Vitruvius 30	14.66	38.00	A	I	13.0	1.20	58.4	2.67	2.3	3.6	B	E	0.9	1.13	140.6	0.03379
Vitruvius 31	14.34	37.16	B	I	7.2	1.23	91.4	0.80	3.0	3.6	A	E	1.0	1.14	79.5	0.02152
Vitruvius 32	14.62	35.42	A	E	4.9	1.22	42.8	0.34	2.2	3.6	A	E~	0.7	1.15	31.6	0.00425
Vitruvius 33	14.32	35.40	A	C~	4.3	1.19	48.6	0.26	2.2	3.6	A	G	0.7	3.32	7.4	–
Vitruvius 34	14.16	35.42	A	C~	4.3	1.12	56.0	0.28	2.5	3.6	A	I	1.2	1.35	109.4	0.04500
Vitruvius 35	14.15	35.61	A	E~	3.8	1.71	56.1	0.29	2.2	3.6	C	–	–	–	–	–
Vitruvius 36	13.96	36.22	A	E~	9.2	1.32	68.0	2.01	2.5	3.6	A	E~	1.5	1.41	191.4	0.13260
Vitruvius 37	13.82	36.35	A	E	3.2	1.70	41.9	0.14	2.5	3.6	B	E~	0.3	1.30	8.4	0.00020
Vitruvius 38	13.74	36.39	A	C~	2.9	1.13	31.2	0.10	2.1	3.6	C	–	–	–	–	–
Vitruvius 39	13.62	36.51	A	E~	7.0	1.56	122.8	1.45	2.9	3.6	A	E	1.5	1.62	121.7	0.07984
Vitruvius 40	13.57	36.71	B	I	5.3	1.11	78.6	0.78	2.7	3.6	B	I	0.7	1.66	16.9	0.00150
Vitruvius 41	13.79	36.97	A	C	6.5	1.08	48.4	0.36	2.4	3.6	A	E	0.5	1.30	35.6	0.00322
Vitruvius 42	13.34	36.77	B	I	11.2	1.38	38.8	1.31	2.3	3.6	A	G	1.7	3.14	143.8	0.13286
Vitruvius 43	13.04	37.45	A	C~	6.5	1.10	57.1	0.61	2.2	3.6	A	E~	0.9	2.07	66.3	0.01158
Vitruvius 44	12.64	37.33	A	I	8.0	1.83	64.1	1.25	2.6	3.6	A	E	1.3	1.89	137.7	0.07114
Vitruvius 45	12.38	37.16	A	E~	5.3	1.27	26.0	0.15	2.3	3.6	B	I	1.0	1.50	43.6	0.00977
Vitruvius 46	12.22	37.36	B	C~	3.6	1.02	25.8	0.09	2.0	3.6	A	C~	0.7	1.20	39.9	0.00582
Vitruvius 47	13.01	35.21	B	I	6.2	1.14	44.3	0.53	2.1	3.6	C	–	–	–	–	–
Vitruvius 48	14.62	33.59	A	C	6.0	1.06	58.9	0.55	2.2	3.6	B	E~	0.5	1.25	10.4	0.00059
Vitruvius 49	14.52	33.28	B	E~	7.4	1.48	47.1	0.75	2.4	3.6	B	C	1.0	1.06	89.1	0.02877
Vitruvius 50	14.02	33.06	B	I	4.2	1.31	31.9	0.16	2.2	3.6	B	G	0.6	2.99	24.6	0.00187
Vitruvius 51	13.71	32.91	B	I	8.3	1.72	43.4	0.78	2.3	3.6	C	–	–	–	–	–
Vitruvius 52	13.59	32.69	A	I	5.2	1.48	21.0	0.13	2.1	3.6	A	E	1.8	1.97	201.7	0.19426

	Mare Dome										Summit Pit Crater					
Name	Lat [°]	Long [°]	Reliability[1]	Shape[2]	Diameter (km)	Ellipticity	Height (m)	Volume (km^3)	Mean slope [°]	Host mare age [Ga]	Reliability[1]	Shape[2]	Diameter (km)	Ellipticity	Depth (m)	Volume (km^3)
Vitruvius 53	13.67	32.59	A	I	5.5	1.22	63.2	0.47	2.2	3.6	A	G	0.8	1.83	29.4	0.00532
Vitruvius 54	15.14	33.00	A	C	4.3	1.02	230.8	1.41	6.4	3.6	C	–	–	–	–	–
Vitruvius 55	15.66	31.92	A	E~	4.3	1.28	88.0	0.51	3.3	3.6	A	E	0.9	1.50	43.9	0.00831
Vitruvius 56	16.21	31.61	A	I	4.3	1.20	94.4	0.58	2.8	3.6	B	C~	0.6	1.28	24.5	0.00192
Vitruvius 57	17.89	30.18	B	C~	21.6	1.15	229.1	27.19	3.1	3.7	B	I	3.4	1.67	276.0	0.70863
Wallach 1	5.45	32.18	A	C~	3.7	1.03	85.5	0.49	3.4	3.6	A	I	0.7	1.65	21.1	0.00248
Wallach 2	5.50	32.11	B	I	2.7	1.56	60.0	0.13	2.8	3.6	B	C	0.8	1.12	58.6	0.00937
Wallach 3	5.47	33.40	A	I	5.6	1.13	70.2	0.69	2.4	3.6	A	C~	1.2	1.02	119.3	0.04869
Wallach 4	4.93	32.97	A	E	3.0	1.19	72.0	0.14	3.0	3.6	A	C~	0.4	1.12	20.4	0.00096
Wallach 5	4.81	33.21	A	I	8.2	1.04	118.2	2.48	3.0	3.6	B	G	0.6	4.36	13.2	–
Wallach 6	4.55	33.24	B	I	4.1	1.35	99.7	0.57	4.1	3.6	A	C~	1.5	1.18	129.7	0.08277
Wallach 7	4.70	33.55	A	E~	5.1	1.33	69.4	0.54	2.5	3.6	B	E	0.7	1.97	22.5	0.00218
Wallach 8	4.52	34.22	A	E~	9.2	1.47	88.5	2.86	3.0	3.6	A	G	0.8	2.81	39.5	0.00300
Wallach 9	4.27	33.84	B	I	5.1	1.49	35.3	0.23	2.4	3.6	C	–	–	–	–	–
Wallach 10	4.02	33.82	A	E~	6.2	1.38	54.0	0.65	2.3	3.6	B	E	0.4	1.30	16.5	–
Wallach 11	4.14	33.56	A	C~	6.5	1.15	98.5	0.87	2.9	3.6	A	E	0.7	1.20	58.3	0.01015
Wallach 12	3.86	33.57	A	E~	10.6	1.50	86.1	3.11	2.5	3.6	B	E	0.7	1.30	38.0	0.00460
Wallach 13	3.60	33.48	B	E	2.9	1.27	35.9	0.07	2.3	3.6	A	E	0.5	1.80	6.1	–
Wallach 14	3.99	32.86	A	E~	4.4	1.33	84.2	0.52	3.5	3.6	B	I	0.4	1.24	4.5	–
Wallach 15	3.98	32.18	A	I	6.6	1.16	39.6	0.30	2.6	3.6	B	C	0.6	1.09	23.9	0.00269
Wallach 16	3.80	31.98	B	I	3.4	1.19	26.3	0.10	2.2	3.6	B	I	0.7	1.81	26.9	0.00141
Wallach 17	4.02	31.99	B	C~	5.3	1.14	39.9	0.33	2.1	3.6	C	–	–	–	–	–
Wallach 18	4.12	30.60	B	I	5.7	1.29	41.2	0.32	2.1	3.6	C	–	–	–	–	–
Wallach 19	4.57	31.04	A	E	5.4	1.43	242.1	2.31	6.4	3.6	B	I	0.8	1.14	47.1	0.00302
Wallach 20	4.70	31.41	A	E	4.5	1.21	32.2	0.13	2.7	3.6	A	E~	0.9	1.21	81.2	0.01742
Wallach 21	4.84	31.12	A	E~	5.5	1.34	81.2	0.92	3.3	3.6	A	I	0.9	1.47	32.3	0.00454
Wallach 22	5.05	31.83	A	E	3.8	1.15	72.7	0.29	2.8	3.6	C	–	–	–	–	–

	Mare Dome										Summit Pit Crater					
Name	Lat [°]	Long [°]	Reliability[1]	Shape[2]	Diameter (km)	Ellipticity	Height (m)	Volume (km^3)	Mean slope [°]	Host mare age [Ga]	Reliability[1]	Shape[2]	Diameter (km)	Ellipticity	Depth (m)	Volume (km^3)
Wallach 23	5.23	31.22	B	I	3.3	1.28	26.2	0.07	2.2	3.6	C	–	–	–	–	–
Wallach 24	5.33	30.84	A	C~	3.9	1.01	97.8	0.34	3.5	3.6	A	I	0.9	1.57	55.9	0.00947
Wallach 25	5.47	31.49	B	E~	4.7	1.47	35.4	0.22	2.2	3.6	C	–	–	–	–	–
Wallach 26	5.69	31.59	A	E~	3.9	1.24	32.8	0.13	1.9	3.6	A	C	0.6	1.20	20.8	0.00165
Wallach 27	6.04	31.67	A	I	4.1	1.20	69.1	0.36	2.6	3.6	C	–	–	–	–	–
Zahringer 1	6.64	40.99	A	C~	6.7	1.13	60.9	0.87	2.9	3.6	A	E~	1.6	1.47	157.2	0.09906
Zahringer 2	6.50	41.23	A	C~	2.8	1.10	52.1	0.12	2.9	3.6	B	C	0.7	1.09	66.7	0.01064
Zahringer 3	4.99	42.09	B	I	3.8	1.40	67.7	0.26	3.1	3.6	A	C	1.0	1.04	105.0	0.02938
Zahringer 4	4.33	41.91	A	C~	5.6	1.15	108.6	1.06	3.2	3.6	C	–	–	–	–	–
Zahringer 5	4.49	41.02	B	E~	5.0	1.25	28.8	0.12	2.1	3.6	A	E	1.0	2.86	47.2	0.01554

[1]Mare dome or summit pit crater identification reliability: A = definite dome structures; B = possible mare dome; C = questionable dome identifications.
[2]Mare dome or summit pit crater shape types: C = circular, E = elliptical, I = irregular, and G = elongated, the tilde ("~") symbol indicate quasi shapes.

5. Characteristics of Mare Domes in Mare Tranquillitatis

5.1 Morphology, Morphometry, and Topography

Representative samples of mare domes of variable identification reliability and shapes are shown in Figure 4. Cauchy 1 represents one of the most well-developed mare dome structures on the Moon (Figures 4A-C), with a nearly perfectly circular base outline ~9 km in diameter. An SLDEM2015-derived topographic profile shows that this dome summit is ~120 m above the adjacent mare, with a clear convex-upward profile (Figure 4C). An apparent elliptical summit pit feature is observed at the top of the dome. Menzel 30 is an example of newly-discovered mare domes reported in this contribution (Figures 4E-F). Due to its very gentle topographic flank slope (2.2 ± 1.5°, measured from SLDEM2015 topography), it is very challenging to detect it from optical imagery data, even on low-Sun images (Figure 4D). High-resolution and high-precision SLDEM2015 topography data clearly identify it as having an approximately circular outline (Figure 4E) and convex profile (Figure 4F). This dome is measured to be 3.7 × 4.2 km in base size and ~104 m in height, and no summit pit feature is observed (Figures 4E and 4F). Many quasi-elliptical domes are also very apparent on the topographic maps (e.g., Vitruvius 10 in Figure 4G). Summit pit features are commonly observed on these elliptical mare domes (e.g., Aryabhata 29 in Figures 4H and 4I), and their presence enhances the identification reliability of the subjacent mare dome. A considerable proportion of our catalogued domes are irregular in outline shape (e.g., Vitruvius 4 in Figure 4J). In some cases, the irregular shape is attributed to the effect of the adjacent pre-existing topography, such as pre-mare highland terrains (such as Menzel 13 in Figures 4K and 4L). Maskelyne 8 (Figures 4M and 4O) is an example of dome features with relatively lower identification reliability (possible domes). It occurs as a raised structure from the background mare, but its irregular outline, being near to other topographic highs, and the absence of a summit pit feature, prevent the confident confirmation of its dome nature. An example of a questionable identification of a mare dome is also shown (Dawes 1 in Figure 4N): image and altimetric data suggest that the raised topography is more likely due to other factors, such as an impact crater ejecta deposit, rather than mare dome formation.

By using the dome base outlines mapped in our data sets (section 4), we build minimum rectangles bounding each dome and measured the length and width of each bounding rectangle as the major and minor axes of the domes (in kilometers), respectively. The geometric mean of the major and minor axes is determined as the dome diameter (Table 1). The base diameters of confirmed mare domes in Mare Tranquillitatis were measured as between ~2 and 23 km (Figure 5A), within the size range of lunar mare domes documented previously (e.g., Head & Gifford, 1980; Wöhler et al., 2006, 2007). (Note that three possible dome features were measured to be over 30 km in diameter, especially Theophilus 1, ~87 km diameter; these are significantly larger than typical mare domes on the Moon.) The histogram of diameters of Tranquillitatis domes is characterized by a unimodal and leptokurtic distribution pattern, peaking at 4–6 km (Figure 5A). The median diameter of Tranquillitatis domes is 5.6 km (n = 283), with ~90% of domes smaller than 12 km. These measurements are smaller than the sizes of global lunar mare dome distributions catalogued previously (Head and Gifford (1980): median diameter 8.0 km, n = 83; Wöhler et al. (e.g., 2006, 2007): median diameter 9.7 km, n = 133), suggesting that our usage of high-resolution (better than 100 m/pixel, Section 2) altimetric and imaging data enables the discovery and characterization of abundant smaller domes.

We also determined the shape of the dome base outlines, including (quasi-)circular, (quasi-)elliptical, and irregular domes, and dome base outline ellipticity (ratio of major to minor axes) (Table 1). We found that most elliptical domes have dome outline ellipticities greater than 1.2, as well as a part of irregularly-outlined domes. The frequency distribution of dome shapes (Figure S3A) shows that Tranquillitatis domes of the three shape types are comparable in quantity. For confirmed mare dome occurrences, circular and elliptical domes are relatively more common than irregular ones, suggesting that these domes are relatively well developed. Domes of lower identification reliability are predominantly irregular in shape, suggesting that their irregular shapes and relationship with other terrains have affected the dome identification procedure. The ellipticity of confirmed mare domes varies between 1.0 and 2.0 (Table 1 and Figure S3B), while several (n = 5) domes of lower identification reliability are more elliptical (ellipticity >2.5). The ellipticity-frequency plot of Tranquillitatis domes shows a leptokurtic distribution, with a positive skewness toward elevated ellipticities, with mean value of 1.29 and median value of 1.24.

We constructed exterior buffer areas around each cataloged dome feature, with a distance of 20% of dome diameter, as the proximal adjacent mare surface (some topographic anomalies, usually relatively large impact craters and dome summit pits, were excluded). The elevation difference between the dome feature and the surrounding mare was calculated from SLDEM2015 topography as the height of each dome. The heights of Tranquillitatis domes range from ~20 m to ~400 m, with a leptokurtic distribution histogram, peaking at 25–70 m (Figure 5B). Domes of lower identification reliability (median height ~53 m) are relatively shorter than confirmed domes (median height ~74 m; Figure 5B). This dome height disparity is clearly observed in the plot of dome height with respect to base diameter (Figure 5C, or height-to-diameter ratio in Figure S3C): height-to-diameter ratio values of confirmed domes vary from 0.004 to ~0.05 (median value of 0.013), while ratios of possible domes are less than ~0.03 (median value of ~0.008). Topographic slope measurements from SLDEM2015 data at a baseline of ~180 m show that dome features in Mare Tranquillitatis are generally very gentle in slope (Figure S3D). The vast majority (268/283 = ~95%) of these domes have average flank slopes between 2° and 4°, confirming that most domes on the Moon are indeed very gently-sloping. Elevated flank slopes (up to ~6°, but still not steep) only occur at a very few dome features.

The calculated volumes of Mare Tranquillitatis domes range over nearly three orders of magnitude, from ~0.05 to nearly 50 km^3, with a median volume 0.7 km^3 (Figure 5D). Smaller volume domes are much more common than larger domes: ~65% of the dome population are less than 1 km^3 in volume (Figure 5D). For domes with volumes less than 1 km^3, the volume-frequency distribution is also concentrated at smaller volumes, peaking between 0.1 and 0.3 km^3 (Figure S3E). (Note that the three possible mare domes with significantly larger sizes mentioned above also have much larger calculated volumes: ranging from two to three orders of magnitude greater than the median volume values.) In addition, the dome volume-diameter plot (Figure S3F) displays an apparent log-linear distribution pattern, especially for confirmed domes, which permits the derivation of an exponential relationship: volume = $0.0867 * e^{0.3356 * \text{diameter}}$ (R^2 = 0.7841), where the volume is in km^3 and the diameter is in km.

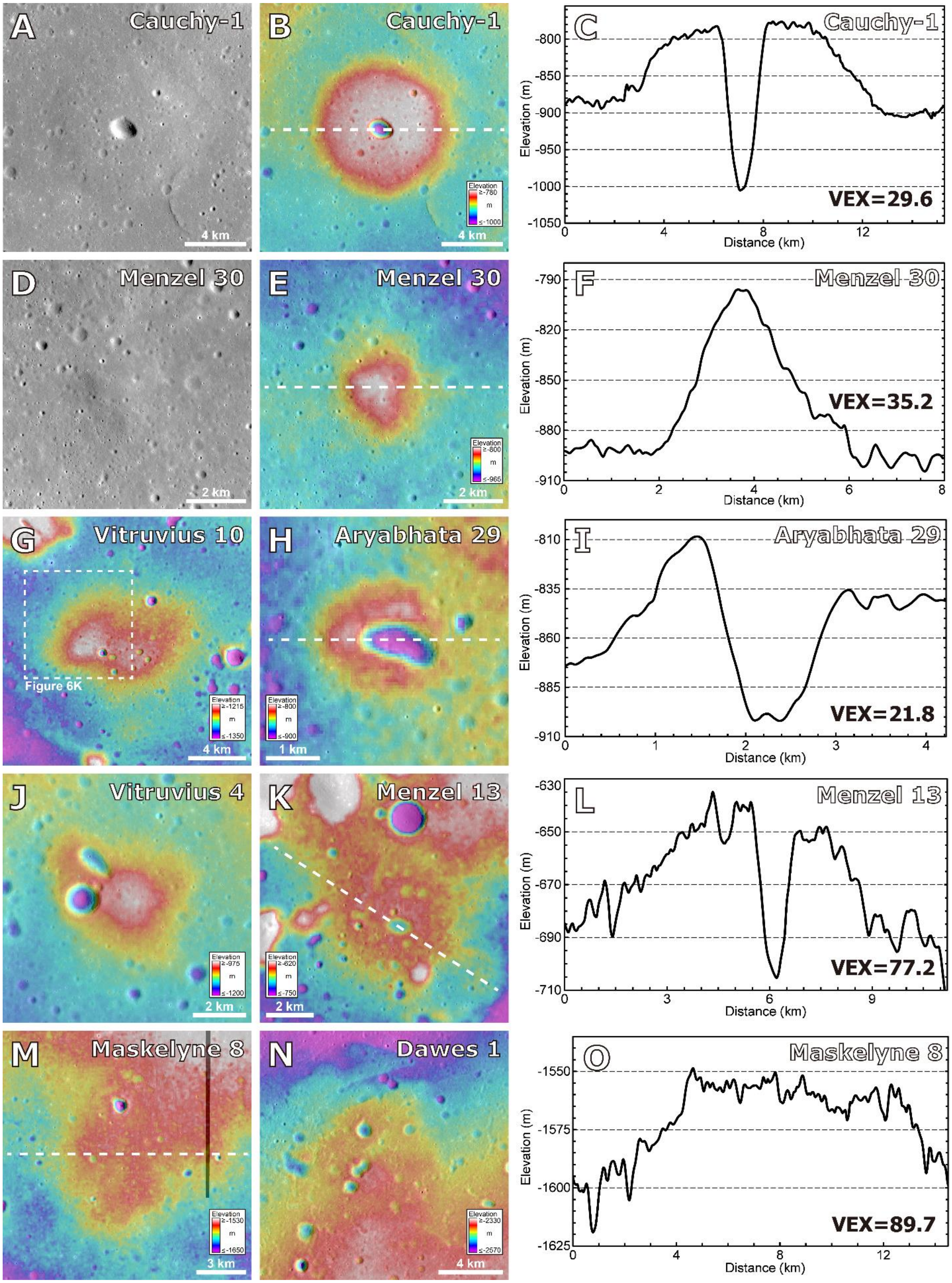
A Cauchy-1
4 km
B Cauchy-1
4 km
C Cauchy-1
VEX=29.6
Elevation (m)
Distance (km)
D Menzel 30
2 km
E Menzel 30
2 km
F Menzel 30
VEX=35.2
G Vitruvius 10
Figure 6K
4 km
H Aryabhata 29
1 km
I Aryabhata 29
VEX=21.8
J Vitruvius 4
2 km
K Menzel 13
2 km
L Menzel 13
VEX=77.2
M Maskelyne 8
3 km
N Dawes 1
4 km
O Maskelyne 8
VEX=89.7

459

Figure 4. Kaguya TC morning images, SLDEM2015 topography maps, and profiles of representative mare domes in Mare Tranquillitatis: (A-C) Cauchy-1, (D-F) Menzel 30, (G) Vitruvius 10 (the dashed white box is the extent of Figure 6K), (H and I) Aryabhata 29, (J) Vitruvius 4, (K and L) Menzel 13, (M and O) Maskelyne 8, and (N) Dawes 1. The locations of topographic profiles (all in a west-east direction) are shown as dashed lines on their respective topographic maps. The vertical exaggeration (VEX) is indicated in each topographic profile.

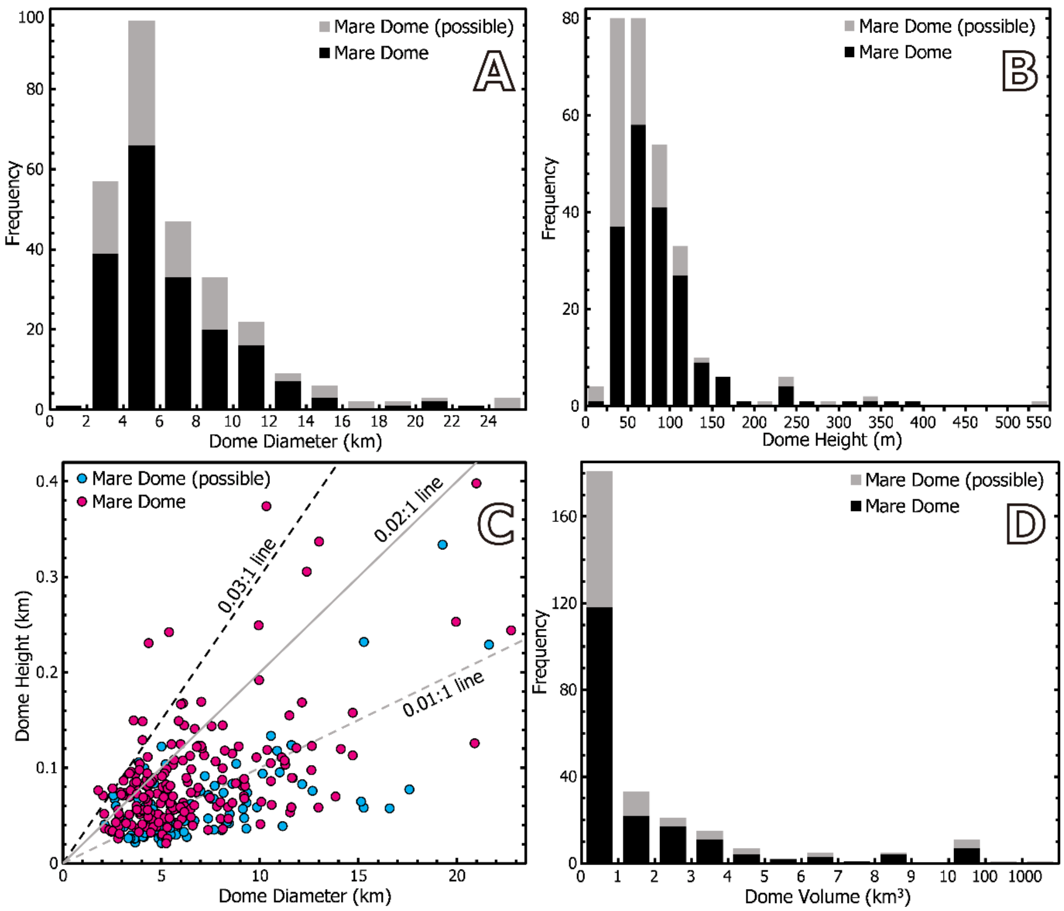

Figure 5. Basic statistics of the main morphometric parameters of mare domes in Mare Tranquillitatis: frequency histograms of (A) dome base outline diameter, (B) dome height relative to the surrounding mare surface and (D) dome volume; (C) plot of dome height against dome base diameter. Note that the three possible domes with unusually large size (>30 km in diameter, Table 1) do not fall within the diameter and height extent of panel C (same for Figures 7B, S3C, S3D, and S3F).

5.2 Summit Pit Craters

Summit pit features are commonly, though not always, observed at the topographic summits of mare domes. These pit craters are important characteristics of the structure of lunar domes, and provide important information for constraining the mechanism of mare dome emplacement. We surveyed the occurrence of summit pits at each catalogued dome feature in Mare Tranquillitatis (Section 4.3 and Figure 3). Among the 283 mare domes, 124 domes are observed to host apparent summit pit features and 85 domes have possible summit pits (lower identification reliability) (Table 1 and Figure S4), revealing that 74% of Tranquillitatis domes are characterized by summit pit features. Summit pits are not observed on 74 catalogued domes in Mare Tranquillitatis (Table 1 and Figure S4). The presence or absence of summit pit features seems to be independent of the diameter, height, and shape of the host mare dome. Both the diameter (median value = 5.6 km, n=209) and height (median value = 71 m) of mare domes that host summit pit features are comparable to those of domes without summit pit features (median diameter = 5.6 km, median height = 58 m, n = 74). The probability of summit pit occurrence is also indistinguishable (all between 70-80%) among mare domes of different base shapes (circular, elliptical, and irregular).

During the summit pit survey procedures, we also determined the outline shape of the summit pit features, including (quasi-)circular, (quasi-)elliptical, (quasi-)elongated, and irregular shapes. The histogram of summit pit occurrences (Figure S5A) shows that an ellipse is the most common shape (~40% of the catalogued 209 summit pit craters); this pattern is different from base shapes of the Tranquillitatis domes, where the three dome shapes are comparable in frequency. A good example of such elliptical summit pits is present on the well-developed Cauchy 1 dome (Figures 4A-C). The pit crater is measured as 1.5 × 1.8 km in size and ~210 m deep below the pit rim, which yields a depth/diameter ratio of ~0.13, comparable with that of relatively fresh lunar impact craters (Type AB or B, Basilevsky, 1976). However, this dome summit pit lacks the raised rim and exterior ejecta deposits typical of fresh lunar impact craters. Distinct summit pits are also observed at the summit of some relatively poorly-developed or irregular mare domes, for instance, Vitruvius 36 (Figure 6A) and Sinas 18 (Figures 6B and 6M). In these cases, the presence of summit pit features helps increase the identification reliability of the host dome. A considerable proportion of the identified summit pits are generally circular in shape (for example, Sinas 1 in Figures 6C and 6N, and Vitruvius 25 in Figure 6D). In a manner similar to the previously mentioned Cauchy 1 summit pit, their unique position at the dome crest and the lack of rim and ejecta still distinguish them from the numerous impact craters on the nearly mare surface (Figures 6C and 6D).

An unusual shape type of dome summit pit is the elongated pit, whose length is generally more than two times its width (e.g., Jansen 7 in Figures 6E and 6O, and Vitruvius 5 in Figure 6F). In addition, some summit pits are irregular in shape (e.g., Menzel 11 in Figure 6G and Maraldi 6 in Figure 6H). In the case of Maraldi 6 summit pit, its irregular shape is mainly due to the extension of the ellipse-shaped pit crater to the northwest. Summit pit crater features are generally centrally located on the dome crest (Figures 6A-H), while some pits are offset from the dome crest (e.g., Aryabhata 4 in Figure 6I). In addition, two or more pit craters are observed to co-occur on tens of mare domes (for instance: Aryabhata 27 in Figure 6J and Vitruvius 10 in Figures 6K and 4G). On the Aryabhata 27 small dome, an elliptical and another irregular pit crater are present on the dome summit and northern flank (near to the dome base), respectively. In the case of Vitruvius 10 dome, a chain of seven small pits, generally circular or elliptical in shape, are aligned from the dome summit to the dome base in a NW-trending direction. An example of a possible summit pit crater is present on the Aryabhata 6 dome (Figure 6L). The small pit indeed occurs at the dome summit position, but its very small size (0.5 × 0.9 km) and shallow depth (~16 m) prevent us from distinguishing it from other depression features, such as topographic irregularities in basaltic lava flows.

In a manner similar to the procedure for morphometric and topographic analyses of mare domes (Section 5.1), we also mapped out the rim positions of dome summit pit features and calculated their size, ellipticity, height, volume, and inner wall slopes. The diameter of mare dome summit pits was estimated to be between ~0.3 and ~3.8 km (Figure 7A). The histogram of summit pit diameter is characterized by a unimodal distribution pattern, peaking at 0.5–1 km, with a median value of 0.8 km. Prior morphometric measurements suggested that dome summit pit diameter (D_c) is correlated with the dome base diameter (D) (Head & Gifford, 1980: $D_c = 0.16 \times D + 0.52$; Wöhler et al., 2006: $D_c = 0.12 \times D + 1.17$). To explore this potential diameter correlation, we plotted the measured diameter of all confirmed (n = 124) and possible (n = 85) summit pit features against the host dome diameter (Figure 7B). The ratio of the summit pit diameter to the dome base diameter varies widely from 0.01 to nearly 0.8, although most (191/209) are between 0.05 to 0.5 (Figures 7B and S5B). However, we did not observe any simple correlation between summit pit diameter and host mare dome diameter: linear fitting of either all summit pits or confirmed pits only yielded correlation coefficients less than 0.3. We suggest that the previously reported correlations are probably biased by their much smaller sampling size, n = 12 (Head & Gifford, 1980) or n = 19 (Wöhler et al., 2016), both over one order of magnitude smaller than our catalogue. The ellipticity of dome summit pit craters shows a much wider range (up to over five; Figure S5C) than that of the host domes (all less than two; Figure S3B), although the majority (~80%) of the summit pits still have ellipticities less than two. The unusually high ellipticity values of summit pits are seen at dozens of elongated pit craters, for instance, Jansen 7 (Figure 6E and ellipticity = 3.9) and Vitruvius 5 (Figure 6F and ellipticity = 2.8).

The depth of summit pits is measured to be between ~4 m to over 600 m, with a skewed distribution, showing that shallower pit craters are more common than deeper ones (Figure 7C). Over 80% of these summit pits are shallower than 100 m. The deepest summit pit crater occurs at the summit of the Jansen 6 small dome, which is elliptical in shape, 2.7 × 4.0 km in size and 626 m deep. Confirmed summit pits (median depth ~54 m) are generally deeper than summit pits of lower identification reliability (median depth ~25 m). The depth/diameter ratio of dome summit pits vary from ~0.01 to ~0.19, with a unimodal histogram distribution pattern peaking at 0.02–0.06 (Figures 7D and S5D). The majority of dome summit pits (84%) have depth/diameter ratios between 0.02 and 0.1 (Figure S5D). Dome summit pits are widely scattered on the diameter-depth plot (Figure 7D) and no simple mathematical relationship can be derived. These statistics of dome summit pit craters are very different from those of meteoritic impact craters of comparable sizes on the Moon. Depending on the degradations state, lunar impact crater depth/diameter ratio generally varies from 0.05 to 0.25 (e.g., Robbins et al., 2018; Stopar et al., 2017). However, about half (52%) of the dome summit pits have depth/diameter ratios smaller than 0.05 (Figure S5D), revealing that a considerable proportion of dome summit pits are significantly shallower than lunar impact craters.

We also found that the bottom of nearly half (46%) of the summit pit craters are topographically lower than the surrounding mare surface (Figure 7E; for instance, Cauchy 1, Aryabhata 29 and Menzel 13 in Figure 4, and Vitruvius 36, Sinas 18, Jansen 7, Vitruvius 5 and Maraldi 6 in Figure 6). This observation is clearly seen from topographic maps and profiles, although not easily perceived from optical images. The summit pit depth relative to the surrounding mare surface seems to be correlated with the summit pit diameter (Figure S5E), suggesting that larger pit diameter may be due to wider feeder dikes, and/or that significant summit pit collapse may occur in larger summit pit craters.

The cavity volume of individual dome summit pit craters varies over five orders of magnitude, from ~10^{-5} to 1.91 km^3, with mean and median volume of 0.051 and 0.005 km^3, respectively (Figure 7F). Nearly half (~43%) of the summit pit craters have cavity volumes between 0.001 and 0.01 km^3. The cavity volume seems to follow a power function of the summit pit diameter: volume = 0.0141*diameter$^{3.3568}$ (fitting for confirmed summit pits, R^2 = 0.8588; Figure S5F), where the volume is in km^3 and the diameter is in km. The maximum topographic slope of the summit pit crater interior wall (also calculated from SLDEM2015 topography at a baseline of ~180 m) ranges from 4 to 36° (Figure S5G), with a median value of 13°. These maximum slopes are comparable to those of the inner walls of lunar impact craters of various degradation states (e.g., Basilevsky, 1976), though dome summit pit craters seem shallower than impact craters. Very steep slopes, steeper or comparable to the angle of repose (32°) of dry materials (such as lunar regolith) are only measured in two dome summit pit craters: one at the summit of Jansen 6 dome, also the deepest summit pit in Mare Tranquillitatis (626 m), and another at the summit of Carrel 8 dome, which is 323 m deep.

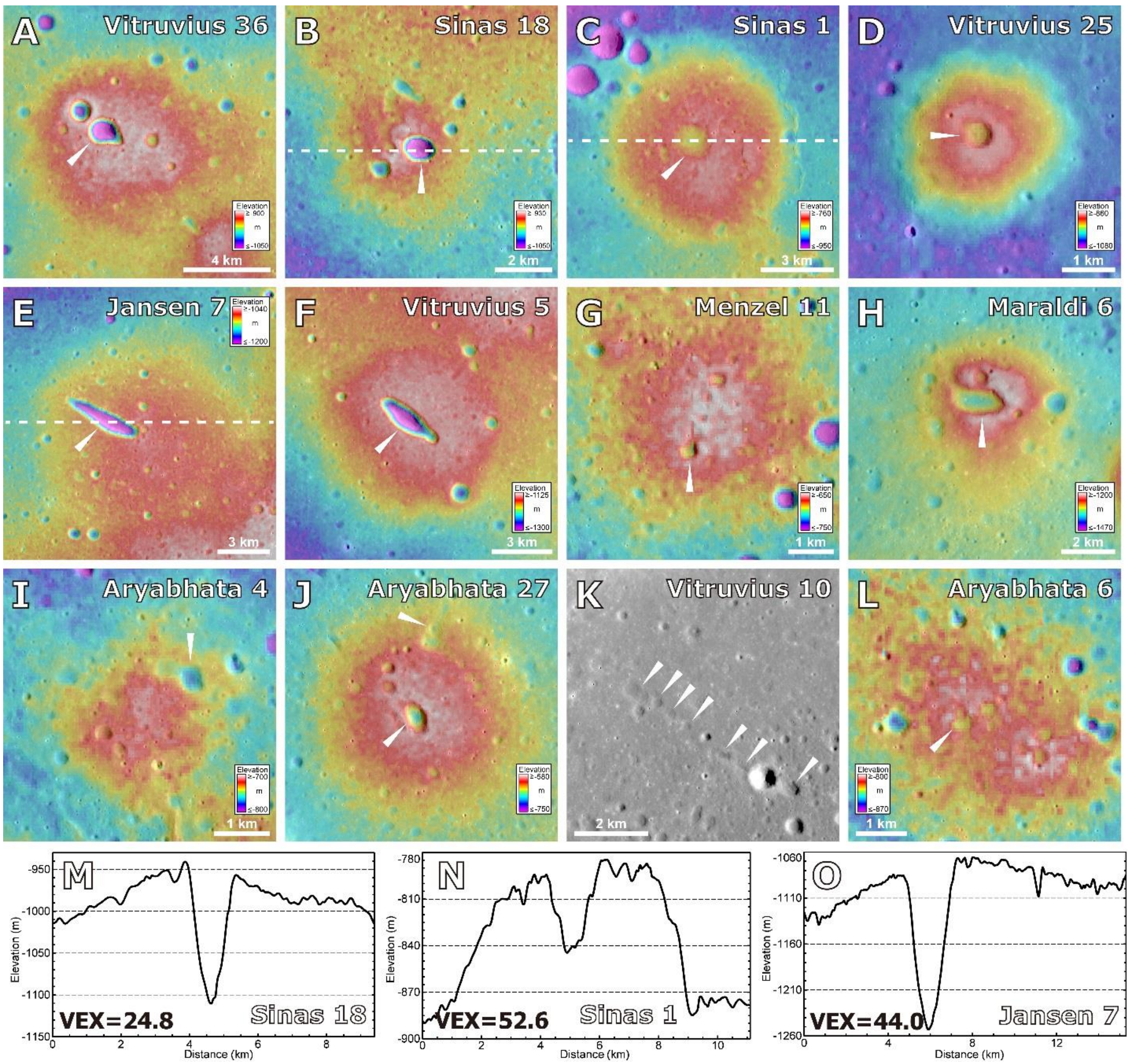

Figure 6. Colorized SLDEM2015 topography overlain on Kaguya TC morning images of representative samples of mare dome summit pit craters in Mare Tranquillitatis: (A) Vitruvius 36, (B) Sinas 18, (C) Sinas 1, (D) Vitruvius 25, (E) Jansen 7, (F) Vitruvius 5, (G) Menzel 11, (H) Maraldi 6, (I) Aryabhata 4, (J) Aryabhata 27, and (L) Aryabhata 6. (K) Kaguya TC image of a chain of pit craters on the Vitruvius 10 dome (see the topographic map of the entire dome in Figure 4G). SLDEM2015 topographic profiles of typical summit pit features: (M) Sinas 18, (N) Sinas 11 (O) Jansen 7; the locations of these profiles (all in a west-east direction) are shown in panels B, C, and E. The vertical exaggeration (VEX) is indicated in each topographic profile.

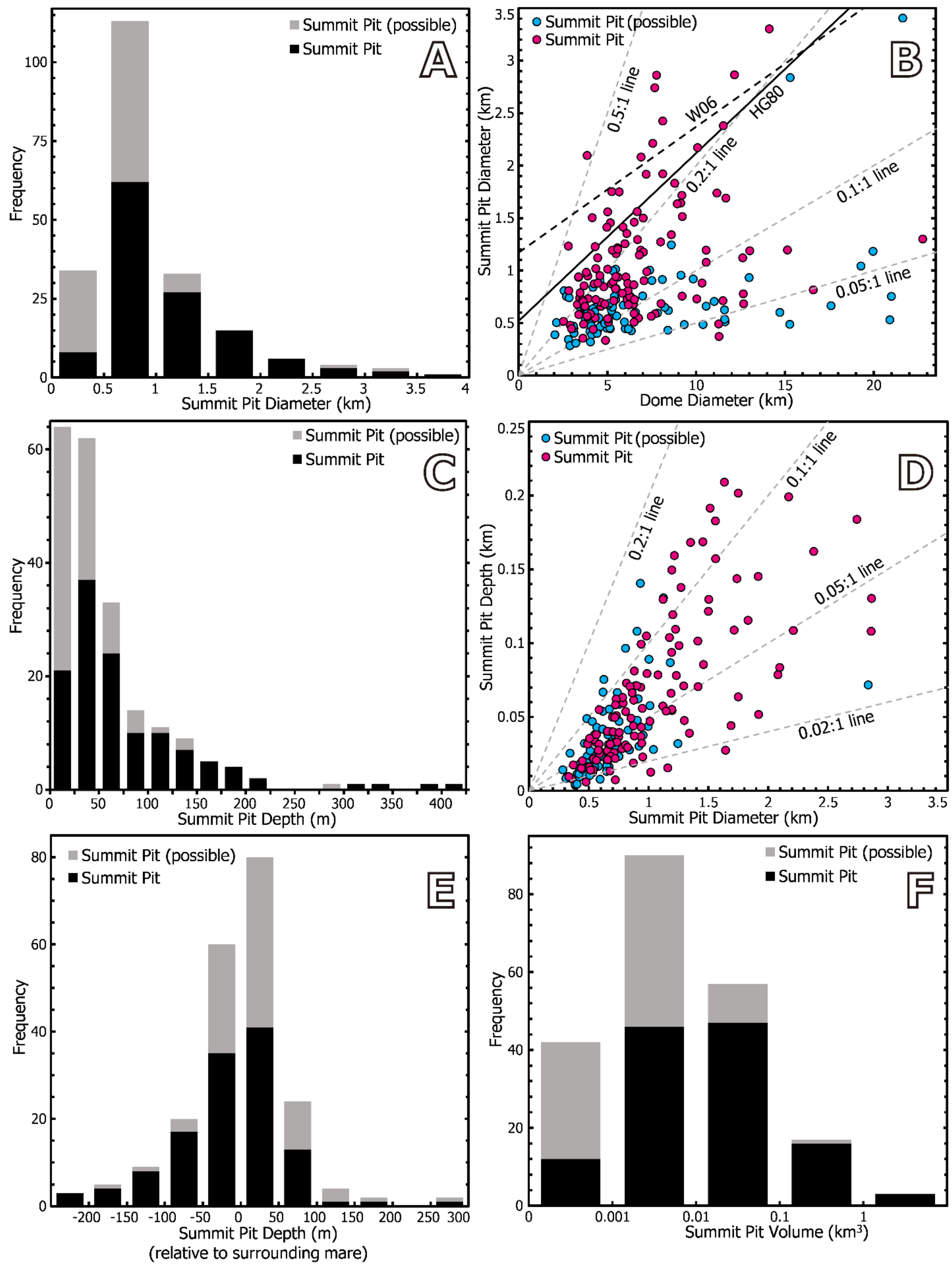

Figure 7. Basic statistics of the main morphometric parameters of mare dome summit pit craters in Mare Tranquillitatis: frequency histograms of summit pit (A) diameter, (C) depth (relative to the summit pit rim), (E) depth relative to the surrounding mare, and (F) cavity volume, and plots of summit pit diameter against (B) host dome diameter and (D) summit pit depth. Note that five summit pits deeper than 0.25 km are not plotted in panel D.

5.3 Chemical Composition

The mare basalts forming Mare Tranquillitatis are characterized by extreme compositional characteristics and significant compositional variations (especially titanium content; Section 3 and Figure 1C). But what are the compositional characteristics of the abundant dome features in Mare Tranquillitatis and how do they compare with those of the surrounding mare basaltic deposits? We calculated the average iron and titanium content of each catalogued mare dome on the basis of FeO and TiO_2 abundance maps derived from Clementine UVVIS (100 m/pixel) and LROC WAC (400 m/pixel) spectrometer data, respectively (Figures 8A, S6A, and S6B). These data show that mare domes in Mare Tranquillitatis are relatively homogeneous in iron content: the vast majority (268/283 = ~95%) of mare domes have average FeO content between 16 and 20 wt.% (Figure S6A). However, the titanium content of Tranquillitatis domes is characterized by considerable variation (Figures 8A and S6B), with average TiO_2 content of individual domes ranging from ~1 to ~11 wt.% (median value = 6.5 wt.%). About 75% of the Tranquillitatis domes have surface TiO_2 content between 4 and 9 wt.%. Although extensive mare basalts in Mare Tranquillitatis (mainly in the northwestern portion) are the most titanium-rich basalts (TiO_2>10 wt.%) on the entire Moon (Figure 1C), high-titanium mare domes are relatively uncommon: only a very small proportion (n = 9 or ~3%) of the domes in Mare Tranquillitatis have average TiO_2 content higher than 10 wt.%. A comparison of the titanium content map (Figure 1C) and the spatial distribution map of mare domes (Figure 3) found that only seven domes and five possible domes occur on or adjacent to the high-titanium basalts in northwestern Mare Tranquillitatis, in an area where the spatial density of mare domes is much lower than in other dome-concentration areas in Mare Tranquillitatis (Figure S2).

We then plotted the iron and titanium contents of each catalogued dome against the composition of the surrounding mare surface (exterior buffer areas with widths of 50% of each dome base diameter) (Figures 8B and 8C). We found that the iron content of mare domes in Mare Tranquillitatis is generally indistinguishable from that of the surrounding mare: the FeO abundance difference between mare domes and their surrounding mare are all within 5% of the surrounding mare FeO content, and the difference is within 3% for 95% (269/283) of these domes (Figure 8B). The titanium content of Mare Tranquillitatis domes, however, shows variations in differences from that of the surrounding mare deposits (Figures 8C and S6C). Though the majority of mare domes (210/283 = 74%) have similar (within ±10%) TiO_2 content to that of the surrounding mare, nearly 30 mare domes show clear TiO_2 content differences from the surrounding mare surface (beyond ±20% of the mare TiO_2 content). Several examples of mare domes with apparently different titanium abundance than the surrounding mare are shown in Figure 9.

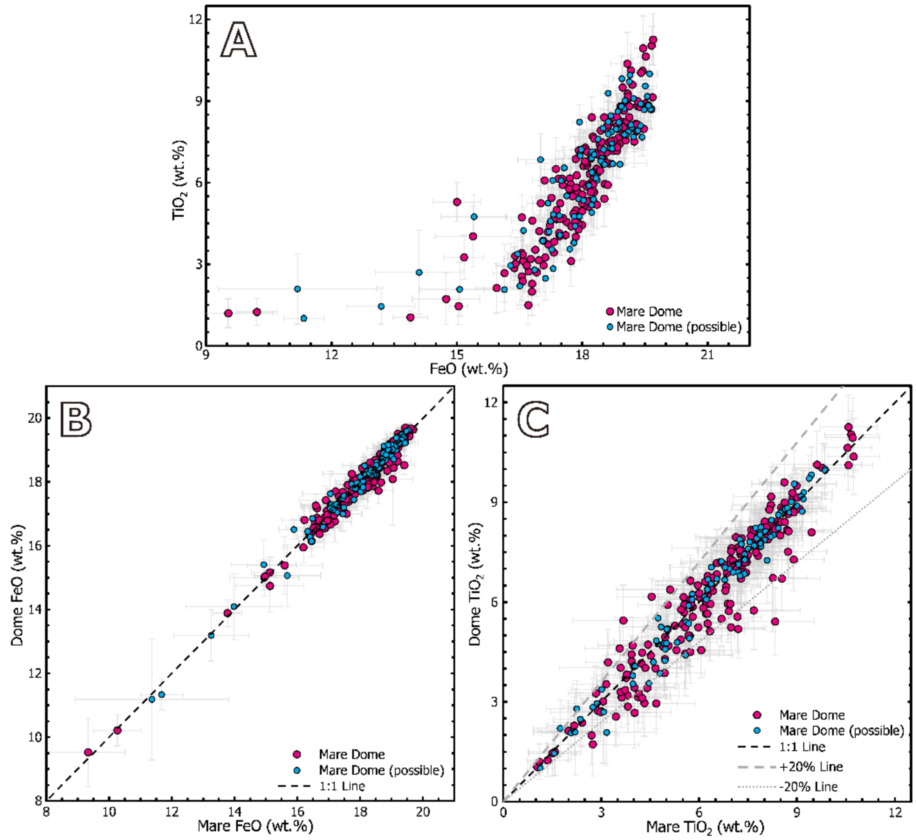

Figure 8. (A) Average iron and titanium content of mare domes in Mare Tranquillitatis, and (B and C) comparison with that of the surrounding mare surface.

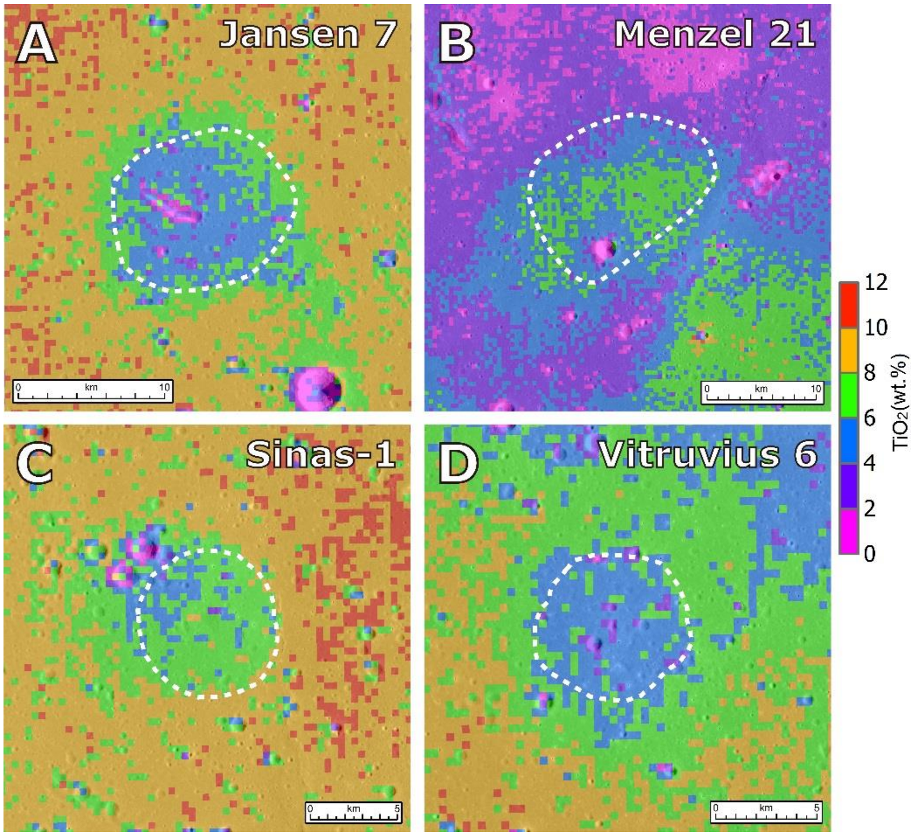

Figure 9. Examples of mare domes (with dome base outlined by dashed lines) in Mare Tranquillitatis with apparently different TiO_2 content compared with the surrounding mare: (A) Jansen 7, (B) Menzel 21, (C) Sinas 1, and (D) Vitruvius 6. Each panel is shown as a WAC-derived TiO_2 content map overlain on a Kaguya TC morning image.

5.4 Ages of the Background Mare Units

Finally, we survey and assess the ages of the mare dome host units in Mare Tranquillitatis. Of the 283 catalogued domes, the background mare units of 273 domes have been dated by the CSFD method, and three domes (Theophilus 1, Vitruvius 11, and Zahringer 4) occur in undated mare units, although adjacent to other dated mare units. Seven domes (Maclear 4 and Maraldi 1-6) are neither on or near any dated mare units; these domes all occur along the northern edges of Mare Tranquillitatis. Overall, 276 domes are located in or near 19 CSFD-dated mare units (Table 1). All but one (Sinas 29, background mare 3.46 Ga) of the mare domes are hosted in mare units that were emplaced more than 3.5 Ga ago (Figure 10A). Compared with the temporal distribution of model ages of global lunar mare units (grey columns in Figure 10B), the ages of dome-hosting mare units (black columns in Figure 10B) are contemporaneous with the peak period of global lunar volcanism, while the background mare ages only span a very narrow temporal range (0.3 Ga), just one tenth of the total duration of extrusive lunar mare volcanism. The identification of abundant mare domes in the most ancient maria strongly supports the hypothesis that small shield-building mare-basalt eruptions may have been a prevalent volcanic eruption style in the earliest stage of lunar volcanism, a potentially very important constraint on lunar thermal evolution history.

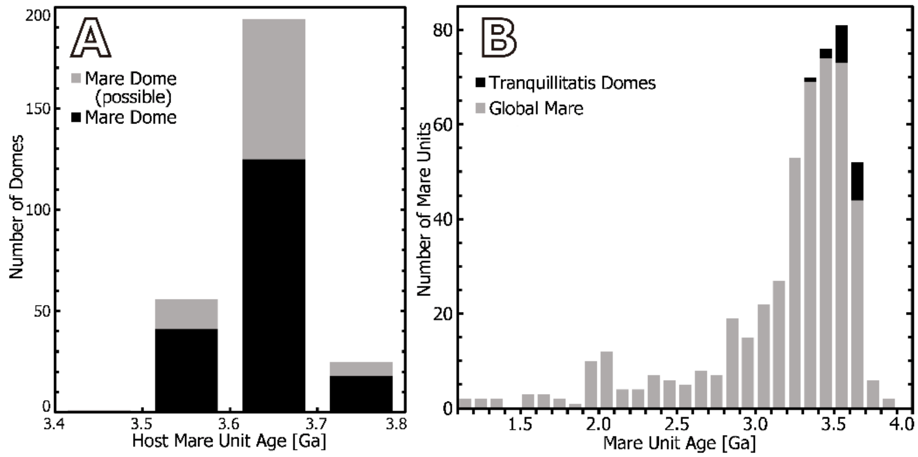

Figure 10. Histogram of host mare unit ages of Tranquillitatis domes counted by (A) the number of dome features and (B) the number of mare units (black columns) in the context of global lunar mare units (grey columns).

6. Discussion and Interpretation

Mare domes, generally interpreted as small shield volcanoes with typical diameters <~30 km (Head & Gifford, 1980), are among the most common types of lunar volcanic source vents (Head & Wilson, 2017). In order to assess their detailed nature and origin, we undertook an extensive analysis of the distribution, nature, associations, and modes of origin of mare domes in Mare Tranquillitatis, known as the location of the highest concentration of mare domes on the Moon (Head & Gifford, 1980; Spudis et al., 2013; Section 4), and one of the oldest lunar maria (~3.5-3.8 Ga; Hiesinger, Head, et al., 2011; Section 3).

6.1 Nature of Small Mare Domes in Mare Tranquillitatis

New high-resolution orbital imaging, topography, and compositional data permitted the documentation of the location and nature of a total of 283 known and suspected mare domes in Mare Tranquillitatis, a significant increase over previous studies (Head & Gifford, 1980; Tye & Head, 2013; Spudis et al., 2013). The Tranquillitatis mare dome population is characterized by a median diameter of 5.6 km, height of 68 m, volume of 0.7 km^3, and ellipticity of 1.2. Summit pits occur in 74% of the population (median pit diameter of 0.8 km, ~14% of mean dome diameter). The deepest pits extend below the level of the surrounding mare surface, and this, together with significant dome ellipticity, suggest the presence of linear source dikes at depth. Mineralogies are dominated by those of intermediate-Ti basalts, and are relatively homogeneous in FeO content, but are variable in TiO_2 content, exhibiting minor variability between the domes and surrounding flow areas. These relationships suggest that the domes both supply and are embayed by flows. Thus, the statistics of dome diameters and heights may be influenced by flooding and embayment by younger lava flows, potentially decreasing diameters and lowering heights.

6.2 Associations of Mare Domes Mare Tranquillitatis

Our detailed regional mapping of Mare Tranquillitatis and the mare dome population revealed that while the region was characterized by an unusual abundance of mare domes, it exhibited a lack or paucity of other features commonly associated with mare basalt source regions and deposits in other parts of the Moon (Head et al., 1981). No evidence for regional dark-mantling deposits, or dark-halo craters of volcanic origin (e.g., Gaddis et al. 2003; Figure S7A) was observed, suggesting that pyroclastic activity was not a major factor in the emplacement of the mare domes. The closest regional dark-mantling deposit occurs in Sulpicius Gallus and at Taurus-Littrow (Apollo 17, Figure S7A), both associated with the edge of the younger Serenitatis impact basin, north of Mare Tranquillitatis. Furthermore, no evidence was observed for dark-halo impact craters (e.g., Figure 6 of Schultz & Spudis, 1979) that might suggest the presence of buried pyroclastic deposits. In addition, we found no evidence for small pyroclastic cones in association with mare domes, dome summit pit craters, or surrounding mare deposits, an association that is common in the Marius Hills in Oceanus Procellarum (e.g., Whitford-Stark & Head, 1977; Lawrence et al., 2013). Taken together, these observations and associations suggest that the volatile content of the magmas that produced the Tranquillitatis domes was low (e.g., Wilson & Head, 2018a), relative to those which produced pyroclastic deposits elsewhere on the Moon.

Two associations suggest that the mare dome magmas may not have been completely devoid of volatiles, however. First, IMPs (Braden et al., 2014; Qiao, Head, Ling, Wilson, 2020), small optically immature features with unusual surface morphologies, were found in association with (within summit pits or on dome flanks) four mare domes (Cauchy 5, Carrell 3, Arago 5 and 7; Figure S7A), most notably Cauchy 5 (Braden et al., 2014; Qiao, Head, Wilson, Ling, 2020). Some workers interpret IMPs to have formed in the last hundred million years (e.g., Braden et al., 2014), and thus to be unrelated in origin to the host mare deposits. Others have interpreted IMPs to be contemporaneous with the host lava flows (Qiao et al., 2017, 2018, 2019; Wilson & Head, 2017b) and, in the case of Cauchy 5 small shield, to be the result of late-stage volatile release and concentration in the final strombolian stages (Wilson & Head, 2017b) of an eruption (e.g., Qiao, Head, Wilson, Ling, 2020). In addition, Zhang et al. (2017, 2020) documented the abundant occurrence (n = 3488) of RMDSs in Mare Tranquillitatis. A considerable proportion (n = 73) of mare domes are observed to have variable numbers of RMDS on their flank, with four domes having over 20 RMDSs (Figure S7B). These small mound features, surrounded by a narrow moat, are found in clusters across the lunar maria and have also been interpreted to be either formed contemporaneously with the host mare unit by second boiling of cooling basalt flows (e.g., Wilson et al., 2019), or emplaced over longer post-host unit time periods, up to the last several hundred million years (e.g., Basilevsky et al., 2019). If the theories of IMP and RMDS origins that suggest formation in association with host lavas are correct, this suggests that at least some of the Tranquillitatis mare dome magmas may have released some volatiles as evidenced by secondary concentration at vent sites and/or in late-stage second boiling in associated lava flows.

We used high-resolution altimetry and topography data to search for lava flow-fronts and estimate their heights. Although regolith thicknesses in mare basalts of this ancient age preclude the ready detection of flow fronts of less than a few meters height, we detected no evidence of flow fronts in excess of a few meters height, for example, comparable to the distinctive 10-30 m high lava flow fronts observed in SW Mare Imbrium (e.g., Schaber, 1973; Bugiolacchi & Guest, 2008; Zhang et al., 2016; Chen et al., 2017), and interpreted to represent very high-volume, high-effusion rate eruptions. The implication is that the Mare Tranquillitatis lava flows are predominantly much thinner, in the range of a few meters, consistent with the flow thickness estimates from the Apollo 11 site in SW Mare Tranquillitatis (Beaty & Albee, 1980) and typical of lower-volume, lower-effusion rate eruptions.

We documented a general lack of sinuous rilles in the interior of Mare Tranquillitatis (Figure S7A), and in association with mare domes, supporting the global studies of Hurwitz et al (2013). The few sinuous depressions that we did observe were narrow, short, and few in number, suggesting that they were more likely to be lava channels than the larger sinuous rilles that are thought to be formed by thermal and mechanical erosion in association with high-volume, high-effusion rate, and long-duration eruptions (e.g., Hurwitz et al., 2013).

We found no evidence for the occurrence of FFCs in Mare Tranquillitatis (Figure S7A), consistent with the findings of Schultz (1976) and Jozwiak et al. (2012). FFCs are evidence of shallow intrusion of large quantities of basaltic magma below impact crater floors, and its associated thermal and volatile evolution (e.g., Wilson & Head, 2018b). The lack of FFCs in Mare Tranquillitatis, together with the absence of calderas, suggests that large-volume shallow sill intrusions and focused magma staging areas were absent in the shallow crust below Mare Tranquillitatis.

In summary, these observations and associations strongly suggest that the eruptions that produced the Tranquillitatis domes were characterized by a large number of individual low-volume, low-volatile content, low-effusion rate, short-duration eruptions. The lack of floor-fractured craters and calderas suggests that shallow sill intrusions and shallow magma staging areas were unimportant. The similarity in morphometry of small shields, their abundance, and high concentration does, however, point to a broad, relatively shallow mantle source region from which many relatively small, similar dike emplacement events originated.

6.3 Implications for Mare Dome Eruption Conditions

These characteristics and associations support the interpretation that the mare domes are small shield volcanoes (Head & Gifford, 1980; Wöhler et al., 2006) that were built from individual low-volume ($<\sim$10-100 km^3), low-volatile content, short-duration, cooling-limited eruptions that formed the shields and supplied lava flows to the immediate surroundings (Head & Wilson, 2017) (Figure 11). These eruption conditions are similar to those of small shields on Earth (e.g., Greeley & King, 1977; Greeley, 1982) which form from low effusion rate episodic eruptions characterized by intermittent supply of magma from sources in the shallow mantle or shallow magma reservoirs in the crust or in a larger edifice (e.g., Iceland, Hawai'i, and the Snake River Plains).

On the Moon (e.g., Wilson & Head, 2017a) magma is predicted to arrive at the surface in dikes at initially relatively higher effusion rates, followed by a decrease in effusion rate with time (Wilson & Head, 2018a; their Fig. 1). For mare domes, initial fissure eruptions from linear dikes penetrating the surface are interpreted to produce relatively more extensive flows, and as the eruption decreases in flux and the vent centralizes (Head & Wilson, 2017; their Fig. 27c), the lower effusion rate causes flows to undergo cooling and become cooling-limited, halting their advance. The succession of cooling-limited flows in the <10 km length range then contributes to the small shield construction. The ellipticities of many shields and shield summit pit craters, and the depths of many pits below the surrounding maria, all support this model and its prediction of a transition, from initial linear dike formation, to fissure eruptions, and finally to small shields with summit pit craters representing eruptions from the centralization of the original linear vent (see Head & Wilson, 2017; their Figs. 13, 17). According to this model, final shield diameter variations are due to small variations in magma cooling and cooling-limited flow lengths. Variations in shield heights may thus be related to eruption duration and total flow volume. Similarities of spectral properties of small shields and surrounding plains documented here and by Wöhler et al. (2006) also support this interpretation. Of course, caution should be exercised in direct application of small shield morphometry in individual shields to eruption conditions, because subsequent adjacent small shield and flow formation may alter the initial shield diameter and height.

The lack of pit craters in some domes is consistent with the predicted relatively low volatile content of the Mare Tranquillitatis small shields. In terrestrial pit craters, the magnitude of floor subsidence and depth is often related to magma withdrawal due to degassing of volatile-rich magmas (e.g., Tilling et al., 1987), and this mechanism has been called upon to explain the characteristics of one of the deepest of the Mare Tranquillitatis pit craters, the Cauchy 5 summit pit crater (e.g., Qiao, Head, Wilson, Ling, 2020). Very low magma volatile contents would minimize such subsidence and the formation of pit craters.

Wöhler et al. (2006) studied over forty domes in four areas of the lunar nearside maria and classified six domes as “lava swells” or intrusive domes (laccoliths) due to the absence of a summit pit crater and their low slopes. Such low-sloped small shield occurrences lacking summit pit craters do not necessarily imply an intrusive origin for the shield; eruptions with lower volatile content could readily lead to lack of a robust strombolian stage and no summit pit crater (e.g., Head & Wilson, 2017). In addition, we found no evidence for the presence of fresh or degraded radial or circumferential cracks that might be produced during a process of intrusion and laccolithic uplift.

Minor occurrences of IMPs on the summits and flanks of some domes, and RMDSs in flanking flows, suggest the presence in a few cases of minor late stage magmatic gas production and concentration (pit craters, Qiao, Head, Wilson, Ling, 2020; and second boiling, Wilson et al., 2019).

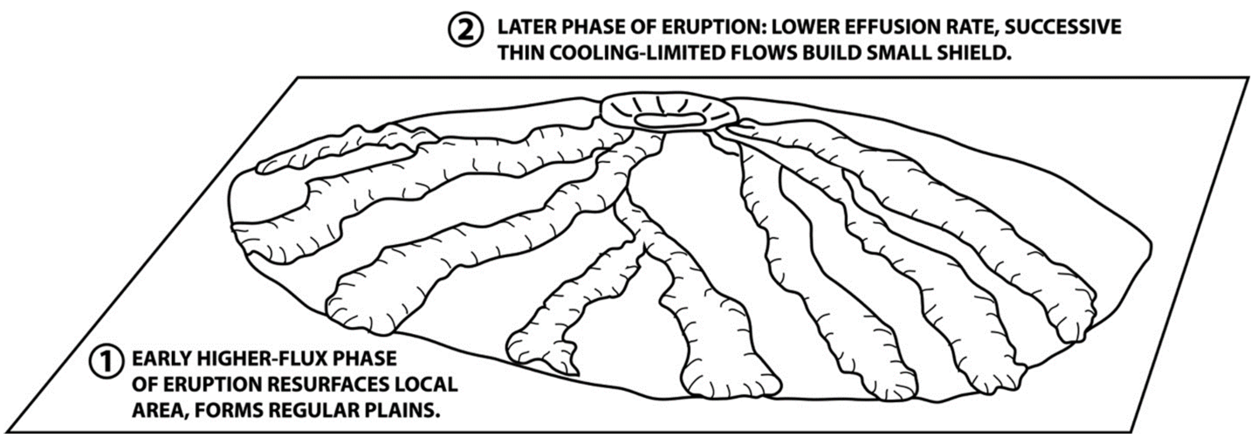

Figure 11. Diagrammatic representation of the sequence of events in the building of small lunar shield volcanoes by cooling limited flows (after Wilson and Head (2017).

6.4 Distribution of Mare Domes in Mare Tranquillitatis and the Style of Volcanism

Our analysis confirmed earlier findings (Head & Gifford, 1980; Spudis et al., 2013; Tye et al., 2013) of a major difference in concentration of mare domes between eastern and western Mare Tranquillitatis, with a very high concentration in eastern Tranquillitatis (Figures 3 and S2). This broad eastern Tranquillitatis concentration formed an ~450 km diameter circular topographic rise (Figure 1B), with several further linear and equidimensional dome clusters within the rise. The rise extends to ~920 m above the surrounding plains, with a corresponding volume of ~1.6×10^5 km^3, and is interpreted to have been built from multiple occurrences of these types of small-shield related eruptions.

This style of eruption characteristic of this broad volcanic rise differs significantly from the flood basalt style of volcanism seen in the younger mascon basins such as Serenitatis, Crisium, and Imbrium, basins that have undergone significant subsidence during their filling, and the very large, long late-stage flows seen in southwest Mare Imbrium (e.g., Schaber, 1973). The eastern Tranquillitatis broad volcanic rise occurrences are most similar to the shield plans volcanism style documented by Greeley (1982) and Greeley and King (1977) in the Snake River Plains of Idaho. Here, fissure eruptions are closely associated with small shield volcanoes and together form vertical accumulations of basaltic plains (Figures 3-12 in Greeley & King, 1977). The broad distribution of the small-shield magma source vents, the very low-rise topography, and the lack of a central caldera in eastern Tranquillitatis support the interpretation of this feature as a broad volcanic rise formed by shield plains style volcanism rather than a large shield volcano as suggested by Spudis et al. (2013).

Implied by the interpretation that the broad volcanic rise was formed by shield plains style volcanism is the presence of a relatively shallow mantle source region capable of supplying distributed dike-emplacement and eruption events forming small shields and associated flanking lava deposits over an area of 1.75×10^5 km^2 for several hundred million years early in mare volcanism history (~3.5-3.8 Ga). These characteristics stand in contrast to western Mare Tranquillitatis, site of similar-aged maria, a broad topographic low, the Lamont mascon and associated tectonic features, and a relative paucity of small shield volcanoes.

We are currently investigating candidate reasons for these stark differences between eastern and western Tranquillitatis, and the younger mascon mare basins. Observed differences in the time, gravity and crustal thickness characteristics, volcanic style, total volumes, and eruption histories may be attributed to the more ancient thermal and crustal structure of the apparently viscously relaxed Tranquillitatis basin, and a shallower broad magma source region present in earlier lunar thermal history due to a thinner lithosphere (e.g., Wilson & Head, 2017a). These results suggest that additional detailed analysis and characterization of volcanic source regions and styles in other lunar maria may provide important evidence for the detailed thermal and magmatic evolution of the Moon.

7. Conclusions

Mare domes, small shield volcanoes typically less than ~30 km in diameter, are part of the spectrum of lunar volcanic source vents (fissures, pits, calderas, dark-halo craters, cones, sinuous rilles, etc.) that characterize extrusive basalt deposits in the lunar maria. We used new spacecraft data to characterize mare domes in Mare Tranquillitatis, among the oldest mare surfaces on the Moon and the site commonly interpreted as an ancient highly morphologically and topographically degraded non-mascon impact basin.

1) We found a total of 283 known and suspected mare domes in Mare Tranquillitatis, with the majority (n = 229) concentrated on a broad, ~450 km diameter circular topographic rise in eastern Tranquillitatis, with several further linear and equidimensional dome clusters within the rise.

2) The mare domes in the Mare Tranquillitatis population are characterized by a median diameter of 5.6 km, height of 68 m, volume of 0.7 km^3, and ellipticity of 1.2. Summit pits occur

in 74% of the population (median pit diameter of 0.8 km, with some pits extending below the level of the surrounding mare surface), supporting an extrusive, rather than intrusive, origin.

3) Detailed mapping revealed an absence of associated calderas, sinuous rilles, cones, and dark mantle/pyroclastic deposits.

4) Compositions are overall relatively homogeneous in FeO content, while variable in TiO_2 content, with minor variability between domes and surrounding flows, suggesting that domes both supply and are embayed by these flows.

5) These characteristics and associations support the interpretation that the mare domes are small shield volcanoes that were built from individual low-volume (<~10-100 km^3), low volatile content, short duration, cooling-limited eruptions that built the shields and supplied lava flows to the immediate surroundings.

6) Minor occurrences of IMPs on the summits and flanks of some domes, and RMDSs in flanking flows, suggest the infrequent presence of minor late stage magmatic gas production and concentration (strombolian activity in pit craters and second boiling in flanking flows).

7) There is a major difference between the distribution of mare domes in eastern and western Mare Tranquillitatis; domes in eastern Tranquillitatis are superposed on a *broad volcanic rise*, ~450 km in diameter, ~920 m high, with a volume of ~1.6×10^5 km^3. We interpret the rise to have been built from multiple occurrences of these types of eruptions, known from terrestrial occurrences as *shield plains volcanism*.

8) The broad distribution of the small-shield magma source vents and the lack of a central caldera support the interpretation of this feature as a *broad volcanic rise* rather than a *large shield volcano*.

9) Implied is a shallow mantle source region capable of supplying distributed dike-emplacement and eruption events over an area of 1.75×10^5 km^2 for several hundred million years early in mare volcanism history (~3.7 Ga). These characteristics stand in contrast to western Tranquillitatis, site of similar-aged maria, the Lamont mascon and associated tectonic features, and a relative paucity of small shield volcanoes.

10) Differences in the time, volcanic style, total volumes, and eruption histories between eastern Tranquillitatis and younger impact basins (e.g., Crisium, Serenitatis, Imbrium mascon basins) are attributed to the more ancient thermal and crustal structure of the apparently viscously relaxed Tranquillitatis basin, and a shallower broad magma source region present in earlier lunar thermal history.

11) These results suggest that additional detailed analysis and characterization of volcanic source regions and styles in other lunar maria may provide important evidence for the detailed thermal and magmatic evolution of the Moon.

Acknowledgments and Data

This study is supported in part by the National Key R&D Program of China (2020YFE0202100), the Pre-research Project on Civil Aerospace Technologies of CNSA (D020204, D020102), National Natural Science Foundation of China (11941001, 41972322) and the China Postdoctoral Science Foundation (2020M682164). J. W. H. gratefully acknowledges financial support for participation in the NASA Lunar Reconnaissance Orbiter Mission Lunar Orbiter Laser

Altimeter (LOLA) Experiment Team (grant 80NSSC19K0605 from the National Aeronautics and Space Administration - Goddard) and from the NASA Lunar Data Analysis Program (80NSSC19K1382). All original LRO data can be found in the NASA Planetary Data System Geosciences Node (https://pds-geosciences.wustl.edu/missions/lro/default.htm) and all original Kaguya/SELENE data are archived at SELENE Data Archive (https://darts.isas.jaxa.jp/planet/pdap/selene/).

References

Andersson, L. E., & Whitaker, E. A. (1982). *NASA catalogue of lunar nomenclature* (NASA reference publication 1097). Washington, DC: National Aeronautics and Space Administration, Scientific and Technical Information Branch.

Barker, M. K., Mazarico, E., Neumann, G. A., Zuber, M. T., Haruyama, J., & Smith, D. E. (2016). A new lunar digital elevation model from the Lunar Orbiter Laser Altimeter and SELENE Terrain Camera. *Icarus*, 273, 346-355. https://doi.org/10.1016/j.icarus.2015.07.039

Basilevsky, A.T., 1976. On the evolution rate of small lunar craters. *Proceedings of the 7th Lunar and Planetary Science Conference*, 1005–1020.

Basilevsky, A. T., Zhang, F., Wöhler, C., Bugiolacchi, R., Head, J. W., & Wilson, L. (2019). Lunar ring-moat dome structures and their relationships with small impact craters. *50th Lunar and Planetary Science Conference*, Lunar and Planetary Institute, The Woodlands, Texas, abstract #1507.

Beaty, D. W., & Albee, A. L. (1978). Comparative petrology and possible genetic relations among the Apollo 11 basalts. *Proceedings of 9th Lunar and Planetary Science*, 359–463.

Beaty D. W., Hill S. M. R., & Albee A. L. (1979). The petrology and chemistry of basaltic fragments from the Apollo 11 soil, part I. *Proceedings of 10th Lunar and Planetary Science*, 41–75.

Beaty, D. W., & Albee, A. L. (1980). The geology and petrology of the Apollo 11 landing site. *Proceedings of the 11th Lunar and Planetary Science Conference*, 23–35.

Boyce, J.M. (1976). Ages of flow units in the lunar nearside maria based on lunar orbiter IV photographs. *Proceedings of 7th Lunar and Planetary Science*, 2717–2728.

Braden, S. E., Stopar, J. D., Robinson, M. S., Lawrence, S. J., van der Bogert, C. H., & Hiesinger, H. (2014), Evidence for basaltic volcanism on the Moon within the past 100 million years. *Nature Geoscience*, 7(11), 787-791. https://doi.org/10.1038/ngeo2252

Bugiolacchi, R., & Guest, J. E. (2008). Compositional and temporal investigation of exposed lunar basalts in the Mare Imbrium region. *Icarus*, 197(1), 1-18. https://doi.org/10.1016/j.icarus.2008.04.001

Carr, M.H. (1966). *Geologic map of the Mare Serenitatis region of the Moon* (Map I-489). U.S. Geological Survey: U.S. Geological Survey.

Chen, Y., Li, C., Ren, X., Liu, J., Wu, Y., Lu, Y., et al. (2018). The thickness and volume of young basalts within Mare Imbrium. *Journal of Geophysical Research: Planets*, 123. https://doi.org/10.1002/2017JE005380

Cho, Y., Morota, T., Haruyama, J., Yasui, M., Hirata, N., & Sugita, S. (2012). Young mare volcanism in the Orientale region contemporary with the Procellarum KREEP Terrane (PKT) volcanism peak period ~2 billion years ago. *Geophysical Research Letters*, 39(11). https://doi.org/10.1029/2012GL051838

De Hon, R. A. (1974). Thickness of mare material in the Tranquillitatis and Nectaris basins. *Proceedings of the 5th Lunar Science*, 53–59.

De Hon, R.A. (2017). A two-basin model for Mare Tranquillitatis, *48th Lunar and Planetary Science Conference*, Lunar and Planetary Institute, The Woodlands, Texas, abstract #2769.

Du, J., Fa, W., Wieczorek, M. A., Xie, M., Cai, Y., & Zhu, M.-H. (2019). Thickness of lunar mare basalts: New results based on modeling the degradation of partially buried craters. *Journal of Geophysical Research: Planets*, 124(9), 2430-2459. https://doi.org/10.1029/2018JE005872

Dvorak, J., & Phillips, R. J. (1979). Gravity anomaly and structure associated with the Lamont region of the moon. *Proceedings of 10th Lunar and Planetary Science*, 2265–2275.

Elston, D. P. (1972). *Geologic map of the Colombo Quadrangle of the Moon* (Map I-714). U.S. Geological Survey: U.S. Geological Survey.

Gaddis, L. R., Staid, M. I., Tyburczy, J. A., Hawke, B. R., & Petro, N. E. (2003). Compositional analyses of lunar pyroclastic deposits. *Icarus*, 161(2), 262-280. https://doi.org/10.1016/S0019-1035(02)00036-2

Greeley, R., & King, J. S. (1977). *Volcanism of the Eastern Snake River Plain, Idaho: A comparative planetary geology guidebook*. Washington, DC: Office of Planetary Geology, National Aeronautics and Space Administration.

Greeley, R. (1982). The Snake River Plain, Idaho: Representative of a new category of volcanism. *Journal of Geophysical Research: Solid Earth*, 87(B4), 2705-2712. https://doi.org/10.1029/JB087iB04p02705

Haruyama, J., Matsunaga, T., Ohtake, M., Morota, T., Honda, C., Yokota, Y., et al. (2008). Global lunar-surface mapping experiment using the Lunar Imager/Spectrometer on SELENE. *Earth, Planets and Space*, 60(4), 243-255. https://doi.org/10.1186/BF03352788

Haruyama, J., Ohtake, M., Matsunaga, T., Morota, T., Honda, C., Yokota, Y., et al. (2009). Long-lived volcanism on the lunar farside revealed by SELENE Terrain Camera. *Science*, 323(5916), 905. https://doi.org/10.1126/science.1163382

Haruyama, J., Hara, S., Hioki, K., Iwasaki, A., Morota, T., Ohtake, M., et al. (2012). Lunar global digital terrain model dataset produced from SELENE (Kaguya) terrain camera stereo observations. *43rd Lunar and Planetary Science Conference*, Lunar and Planetary Institute, The Woodlands, Texas, abstract #1200.

Head, J. W., & Lloyd, D. D. (1971). Near-terminator photography. In *Apollo 14 Preliminary Science Report* (NASA SP-272, pp. 297-300). Washington, DC: United States Government Printing Office.

Head, J. W., & Gifford, A. (1980). Lunar mare domes: Classification and modes of origin. *The Moon and the Planets*. 22, 235-258. https://doi.org/doi:10.1007/BF00898434

Head, J. W., Sparks, R. S., Bryan, W. B., Walker, G. P. L., Greeley, R., Whitford-Stark, J. L., et al. (1981). Distribution and morphology of basalt deposits on planets. In *Basaltic Volcanism on the Terrestrial Planets* (pp. 701–800). New York: Pergamon Press Inc.

Head, J. W., & Wilson, L. (2017). Generation, ascent and eruption of magma on the Moon: New insights into source depths, magma supply, intrusions and effusive/explosive eruptions (Part 2: Predicted emplacement processes and observations). *Icarus*, 283, 176-223. https://doi.org/10.1016/j.icarus.2016.05.031

Hiesinger, H., Jaumann, R., Neukum, G., & Head III, J. W. (2000). Ages of mare basalts on the lunar nearside. *Journal of Geophysical Research: Planets*, 105(E12), 29239-29275. https://doi.org/10.1029/2000JE001244

Hiesinger, H., Head, J. W., III, Wolf, U., Jaumann, R., & Neukum, G. (2006). New ages for basalts in Mare Fecunditatis based on crater size-frequency measurements. *37th Lunar and Planetary Science Conference*. Lunar and Planetary Institute, The Woodlands, Texas, abstract #1151.

Hiesinger, H., Head, J. W., Wolf, U., Jaumann, R., & Neukum, G. (2011). Ages and stratigraphy of lunar mare basalts: A synthesis. *Geological Society of America Special Papers*, 477, 1-51. https://doi.org/10.1130/2011.2477(01)

Hiesinger, H., van der Bogert, C. H., Reiss, D., & Robinson, M. S. (2011). Crater size-frequency distribution measurements of Mare Crisium. *42th Lunar and Planetary Science Conference*. Lunar and Planetary Institute, The Woodlands, Texas, abstract #2179.

Hurwitz, D. M., Head, J. W., & Hiesinger, H. (2013). Lunar sinuous rilles: Distribution, characteristics, and implications for their origin. *Planetary and Space Science*, 79-80, 1-38. https://doi.org/10.1016/j.pss.2012.10.019

Jamieson, H. D. & Rae, W. L. (1965). The joint A.L.P.O. – B.A.A. lunar dome project. *Journal of the British Astronomical Association*, 75, 310-314.

Jerde, E. A., Snyder, G. A., Taylor, L. A., Yun-Gang, L., & Schmitt, R. A. (1994). The origin and evolution of lunar high-Ti basalts: Periodic melting of a single source at Mare Tranquillitatis. *Geochimica et Cosmochimica Acta*, 58(1), 515-527. https://doi.org/10.1016/0016-7037(94)90480-4

Jozwiak, L. M., Head, J. W., Zuber, M. T., Smith, D. E., & Neumann, G. A. (2012). Lunar floor-fractured craters: Classification, distribution, origin and implications for magmatism and shallow crustal structure. *Journal of Geophysical Research: Planets*, 117(E11). https://doi.org/10.1029/2012JE004134

Korotev, R. L., & Irving, A. J. (2021). Lunar meteorites from northern Africa. *Meteoritics & Planetary Science*, in press. https://onlinelibrary.wiley.com/doi/abs/10.1111/maps.13617

Kreslavsky, M. A., Head, J. W., Neumann, G. A., Zuber, M. T., & Smith, D. E. (2017). Low-amplitude topographic features and textures on the Moon: Initial results from detrended Lunar Orbiter Laser Altimeter (LOLA) topography. *Icarus*, 283, 138-145. http://dx.doi.org/10.1016/j.icarus.2016.07.017

Lawrence, S. J., Stopar, J. D., Hawke, B. R., Greenhagen, B. T., Cahill, J. T. S., Bandfield, J. L., et al. (2013). LRO observations of morphology and surface roughness of volcanic cones and lobate lava flows in the Marius Hills. *Journal of Geophysical Research-Planets*, 118(4), 615-634. https://doi.org/10.1002/jgre.20060

Lena, R., Wöhler, C., Phillips, J., Wirths, M., & Bregante, M. T. (2007). Lunar domes in the Doppelmayer region: Spectrophotometry, morphometry, rheology, and eruption conditions. *Planetary and Space Science*, 55(10), 1201-1217. https://doi.org/10.1016/j.pss.2007.01.007

Lloyd, D. D., Head, J. W., 1972. Lunar surface properties as determined from earth-shine and near-terminator photography. *Proceedings of 3rd Lunar and Planetary Science*, 3127-3142.

LSPET (Lunar Sample Preliminary Examination Team) (1969), Preliminary examination of lunar samples. In *Apollo 11 Preliminary Science Report* (NASA SP-214, pp. 123-142). Washington, DC: United States Government Printing Office.

Lucey, P. G., Blewett, D. T., & Hawke, B. R. (1998). Mapping the FeO and TiO_2 content of the lunar surface with multispectral imagery. *Journal of Geophysical Research*, 103(E2), 3679-3699. http://dx.doi.org/10.1029/97JE03019

Lucey, P. G., Blewett, D. T., & Jolliff, B. L. (2000). Lunar iron and titanium abundance algorithms based on final processing of Clementine ultraviolet-visible images. *Journal of Geophysical Research: Planets*, 105(E8), 20297-20305. https://doi.org/10.1029/1999je001117

McKay, D. S., Heiken, G., Basu, A., Blanford, G., Simon, S., Reedy, R., et al. (1991). The lunar regolith. In G. H. Heiken, D. T. Vaniman & B. M. French (Eds.), *Lunar sourcebook* (pp. 285-356). Cambridge: Cambridge University Press.

Milton, D.J. (1968), *Geologic map of the Theophilus Quadrangle of the Moon* (Map I-546). U.S. Geological Survey: U.S. Geological Survey.

Morota, T., Haruyama, J., Honda, C., Ohtake, M., Yokota, Y., Kimura, J., et al. (2009). Mare volcanism in the lunar farside Moscoviense region: Implication for lateral variation in magma production of the Moon. *Geophysical Research Letters*, 36(21). https://doi.org/10.1029/2009GL040472

Morota, T., Haruyama, J., Ohtake, M., Matsunaga, T., Honda, C., Yokota, Y., et al. (2011). Timing and characteristics of the latest mare eruption on the Moon. *Earth and Planetary Science Letters*, 302(3–4), 255-266. https://doi.org/10.1016/j.epsl.2010.12.028

Morris, E.C., and D. E. Wilhelms (1967), *Geologic map of the Julius Caesar Quadrangle of the Moon* (Map I-510). U.S. Geological Survey: U.S. Geological Survey.

National Research Council (2007). *The scientific context for exploration of the Moon*. Washington DC: National Academies Press.

Nelson, D. M., Koeber, S. D., Daud, K., Robinson, M. S., Watters, T. R., Banks, M. E., & Williams, N. R. (2014). Mapping lunar maria extents and lobate scarps using LROC image products. *45th Lunar and Planetary Science Conference*. Lunar and Planetary Institute, The Woodlands, Texas, abstract #2961.

Neumann, G. A., Zuber, M. T., Wieczorek, M. A., Head, J. W., Baker, D. M. H., Solomon, S. C., et al. (2015). Lunar impact basins revealed by Gravity Recovery and Interior Laboratory measurements. *Science Advances*, 1(9), e1500852. https://doi.org/10.1126/sciadv.1500852

Pasckert, J. H., Hiesinger, H., & van der Bogert, C. H. (2015). Small-scale lunar farside volcanism. *Icarus*, 257, 336-354. http://dx.doi.org/10.1016/j.icarus.2015.04.040

Pasckert, J. H., Hiesinger, H., & van der Bogert, C. H. (2018). Lunar farside volcanism in and around the South Pole–Aitken basin. *Icarus*, 299(Supplement C), 538-562. https://doi.org/10.1016/j.icarus.2017.07.023

Pieters, C. M. (1978). Mare basalt types on the front side of the Moon: A summary of spectral reflectance data. *Proceedings of 9th Lunar and Planetary Science*, 2825–2849.

Qiao, L., Head, J., Wilson, L., Xiao, L., Kreslavsky, M., & Dufek, J. (2017). Ina pit crater on the Moon: Extrusion of waning-stage lava lake magmatic foam results in extremely young crater retention ages. *Geology*, 45(5), 455-458. https://doi.org/10.1130/G38594.1

Qiao, L., Head, J. W., Xiao, L., Wilson, L., & Dufek, J. D. (2018). The role of substrate characteristics in producing anomalously young crater retention ages in volcanic deposits on the Moon: Morphology, topography, sub-resolution roughness and mode of emplacement of the Sosigenes Lunar Irregular Mare Patch (IMP). *Meteoritics & Planetary Science*, 53(4), 778-812. https://doi.org/10.1111/maps.13003.

Qiao, L., Head, J. W., Ling, Z., Wilson, L., Xiao, L., Dufek, J. D., & Yan, J. (2019). Geological characterization of the Ina shield volcano summit pit crater on the Moon: Evidence for extrusion of waning-stage lava lake magmatic foams and anomalously young crater retention ages. *Journal of Geophysical Research: Planets*, 124(4), 1100-1140. https://doi.org/10.1029/2018JE005841

Qiao, L., Head, J. W., Ling, Z., & Wilson, L. (2020). Lunar irregular mare patches: Classification, characteristics, geologic settings, updated catalog, origin, and outstanding questions. *Journal of Geophysical Research: Planets*, 125(7), e2019JE006362. https://doi.org/10.1029/2019JE006362

Qiao, L., Head, J. W., Wilson, L., & Ling, Z. (2020). The Cauchy 5 small, low-volume lunar shield volcano: Evidence for volatile exsolution-eruption patterns and type 1/type 2 hybrid irregular mare patch formation. *Journal of Geophysical Research: Planets*, 125(2), e2019JE006171. https://doi.org/10.1029/2019JE006171

Rae, W. L. (1966). Lunar domes. *Journal of the British Astronomical Association*, 76, 319-327.

Robbins, S. J., Watters, W. A., Chappelow, J. E., Bray, V. J., Daubar, I. J., Craddock, R. A., et al. (2018). Measuring impact crater depth throughout the solar system. *Meteoritics & Planetary Science*, 53(4), 583-637. https://doi.org/10.1111/maps.12956

Robinson, M. S., Brylow, S. M., Tschimmel, M., Humm, D., Lawrence, S. J., Thomas, P. C., et al. (2010). Lunar Reconnaissance Orbiter Camera (LROC) instrument overview. *Space Science Reviews*, 150(1), 81-124. https://doi.org/10.1007/s11214-010-9634-2

Salisbury, J. W. (1961). The origin of lunar domes. *The Astrophysical Journal*, 134, 126–129.

Sato, H., Robinson, M. S., Lawrence, S. J., Denevi, B. W., Hapke, B., Jolliff, B. L., & Hiesinger, H. (2017). Lunar mare TiO_2 abundances estimated from UV/Vis reflectance. *Icarus*, 296, 216-238. https://doi.org/10.1016/j.icarus.2017.06.013

Schaber, G. G. (1973). Lava flows in Mare Imbrium: Geologic evaluation from Apollo orbital photography. *Proceedings of the 4th Lunar and Planetary Science* (Vol. 1), 73-92.

Schultz, P. H. (1976). Floor-fractured lunar craters. *The moon*, 15(3), 241-273. https://doi.org/10.1007/BF00562240

Schultz, P. H., & Spudis, P. D. (1979). Evidence for ancient mare volcanism. *Proceedings of 10th Lunar and Planetary Science Conference*, 2899-2918.

Scott, D. H., & H. A. Pohn (1972), *Geologic map of the Macrobius quadrangle of the Moon* (Map I-799). U.S. Geological Survey: U.S. Geological Survey.

Shearer, C. K., Hess, P. C., Wieczorek, M. A., Pritchard, M. E., Parmentier, E. M., Borg, L. E., et al. (2006). Thermal and magmatic evolution of the Moon. *Reviews in mineralogy and geochemistry*, 60(1), 365-518. https://doi.org/10.2138/rmg.2006.60.4

Smith, E. I. (1973). Identification, distribution and significance of lunar volcanic domes. *The Moon*, 6, 3-31. https://doi.org/10.1007/BF02630650

Smith, D. E., Zuber, M. T., Jackson, G. B., Cavanaugh, J. F., Neumann, G. A., Riris, H., et al. (2010). The Lunar Orbiter Laser Altimeter investigation on the Lunar Reconnaissance Orbiter mission. *Space Science Reviews*, 150(1), 209-241. https://dx.doi.org/10.1007/s11214-009-9512-y

Snape, J. F., Nemchin, A. A., Whitehouse, M. J., Merle, R. E., Hopkinson, T., & Anand, M. (2019). The timing of basaltic volcanism at the Apollo landing sites. *Geochimica et Cosmochimica Acta*, 266, 29-53. https://doi.org/10.1016/j.gca.2019.07.042

Solomon, S. C., Comer, R. P., & Head, J. W. (1982). The evolution of impact basins: Viscous relaxation of topographic relief. *Journal of Geophysical Research: Solid Earth*, 87(B5), 3975-3992. https://doi.org/10.1029/JB087iB05p03975.

Spudis, P. D. (1993). *The geology of multi-ring impact basins*, Cambridge: Cambridge University Press.

Spudis, P.D. (2015). Volcanism on the Moon. In: H. Sigurdsson, B. Houghton, S.R., Rymer, H. Rymer, J. Stix (Eds.), *Encyclopedia of Volcanoes* (2nd edition, pp. 697-708). New York: Academic Press.

Spudis, P. D., McGovern, P. J., & Kiefer, W. S. (2013). Large shield volcanoes on the Moon. *Journal of Geophysical Research: Planets*, 118(5), 1063-1081. https://doi.org/10.1002/jgre.20059

Spurr, J.E. (1945). *Geology Applied to Selenology* (Books I and II). Lancaster: Science Press.

Staid, M. I., Pieters, C. M., & Head, J. W. (1996). Mare Tranquillitatis: Basalt emplacement history and relation to lunar samples. *Journal of Geophysical Research: Planets*, 101(E10), 23213-23228. https://doi.org/10.1029/96JE02436

Stopar, J. D., Robinson, M. S., Barnouin, O. S., McEwen, A. S., Speyerer, E. J., Henriksen, M. R., & Sutton, S. S. (2017). Relative depths of simple craters and the nature of the lunar regolith. *Icarus*, 298, 34-48. https://doi.org/10.1016/j.icarus.2017.05.022

Tilling, R. I., Christiansen, R. I., Duffield, W. A., Endo, E. T., Holcomb, R. T., Koyanagi, R. Y., Peterson, D. W., & Unger, J. D. (1987). The 1972–1974 Mauna Ulu eruption, Kilauea volcano: An example of quasi-steady-state magma transfer, In R. W. Decker, T. L. Wright, & P. H. Stauffer (Eds.), *Volcanism in Hawaii*, U.S. Geological Survey Professional Paper 1350 (pp. 405–469). Washington: United States Government Printing Office.

Tye, A. R., & Head, J. W. (2013). Mare Tranquillitatis: Distribution of mare domes, relation to broad mare rise, and evidence of a previously unrecognized basin from LOLA altimetric data. *44rd Lunar and Planetary Science Conference*, Lunar and Planetary Institute, The Woodlands, Texas, abstract #1319.

Tyrie, A. (1988). Age dating of mare in the lunar crater Tsiolkovsky by crater-counting method. *Earth, Moon, and Planets*, 42(3), 245-264. https://doi.org/10.1007/BF00058489

Whitford-Stark, J. L., & Head, J. W. (1977). The Procellarum volcanic complexes: Contrasting styles of volcanism, *Proceedings of 8th Lunar Science Conference*, 2705–2724.

Whitten, J., Head, J. W., Staid, M., Pieters, C. M., Mustard, J., Clark, R., et al. (2011). Lunar mare deposits associated with the Orientale impact basin: New insights into mineralogy, history, mode of emplacement, and relation to Orientale Basin evolution from Moon Mineralogy Mapper (M^3) data from Chandrayaan-1. *Journal of Geophysical Research: Planets*, 116(E6). https://doi.org/10.1029/2010JE003736

Wieczorek, M. A., Jolliff, B. L., Khan, A., Pritchard, M. E., Weiss, B. P., Williams, J. G., et al. (2006). The constitution and structure of the lunar interior. *Reviews in mineralogy and geochemistry*, 60(1), 221-364. https://doi.org/10.2138/rmg.2006.60.3

Wilhelms, D.E. (1972). *Geologic map of the Taruntius quadrangle of the Moon* (Map I-722). U.S. Geological Survey: U.S. Geological Survey.

Wilhelms, D.E. (1987). *The Geological History of the Moon* (U.S. Geological Survey Professional Paper 1384). Washington D.C.: United States Government Printing Office.

Wilson, L., & Head, J. W. (2017a). Generation, ascent and eruption of magma on the Moon: New insights into source depths, magma supply, intrusions and effusive/explosive eruptions (Part 1: Theory). *Icarus*, 283, 146-175. https://doi.org/10.1016/j.icarus.2015.12.039

Wilson, L., & Head, J. W. (2017b). Eruption of magmatic foams on the Moon: Formation in the waning stages of dike emplacement events as an explanation of "irregular mare patches". *Journal of Volcanology and Geothermal Research*, 335, 113-127. https://doi.org/10.1016/j.jvolgeores.2017.02.009

Wilson, L., & Head, J. W. (2018a). Controls on lunar basaltic volcanic eruption structure and morphology: Gas release patterns in sequential eruption phases. *Geophysical Research Letters*, 45(12), 5852-5859. https://doi.org/10.1029/2018GL078327

Wilson, L., & Head, J. W. (2018b). Lunar floor-fractured craters: Modes of dike and sill emplacement and implications of gas production and intrusion cooling on surface morphology and structure. *Icarus*, 305, 105-122. https://doi.org/10.1016/j.icarus.2017.12.030

Wilson, L., Head, J. W., & Zhang, F. (2019). A theoretical model for the formation of Ring Moat Dome Structures: Products of second boiling in lunar basaltic lava flows. *Journal of Volcanology and Geothermal Research*, 374, 160-180. https://doi.org/10.1016/j.jvolgeores.2019.02.018

Wöhler, C., Lena, R., Lazzarotti, P., Phillips, J., Wirths, M., & Pujic, Z. (2006). A combined spectrophotometric and morphometric study of the lunar mare dome fields near Cauchy, Arago, Hortensius, and Milichius. *Icarus*, 183(2), 237-264. https://doi.org/10.1016/j.icarus.2006.03.003

Wöhler, C., Lena, R., & Phillips, J. (2007). Formation of lunar mare domes along crustal fractures: Rheologic conditions, dimensions of feeder dikes, and the role of magma evolution. *Icarus*, 189(2), 279-307. https://doi.org/10.1016/j.icarus.2007.01.011

Wöhler, C., Lena, R., Group, G.L.R.G., 2009. Lunar intrusive domes: Morphometric analysis and laccolith modelling. *Icarus* 204, 381-398.

Zhang, F., Zhu, M. H., & Zou, Y. L. (2016). Late stage Imbrium volcanism on the Moon: Evidence for two source regions and implications for the thermal history of Mare Imbrium. *Earth and Planetary Science Letters*, 445, 13-27. https://doi.org/10.1016/j.epsl.2016.04.003

Zhang, F., Head, J. W., Basilevsky, A. T., Bugiolacchi, R., Komatsu, G., Wilson, L., et al. (2017). Newly discovered ring-moat dome structures in the lunar maria: Possible origins and implications. *Geophysical Research Letters*, 44(18), 9216-9224. http://dx.doi.org/10.1002/2017GL074416

Zhang, F., Head, J. W., Wöhler, C., Bugiolacchi, R., Wilson, L., Basilevsky, A. T., et al. (2020). Ring-moat dome structures (RMDSs) in the lunar Maria: Statistical, compositional, and morphological characterization and assessment of theories of origin. *Journal of Geophysical Research: Planets*, 125, e2019JE005967. https://doi.org/10.1029/2019JE005967

Zuber, M. T., Smith, D. E., Watkins, M. M., Asmar, S. W., Konopliv, A. S., Lemoine, F. G., et al. (2013). Gravity Field of the Moon from the Gravity Recovery and Interior Laboratory (GRAIL) Mission. *Science*, 339(6120), 668-671. https://doi.org/10.1126/science.1231507

AGU PUBLICATIONS

Journal of Geophysical Research: Planets

Supporting Information for

Mare Domes in Mare Tranquillitatis: Identification, Characterization, and Implications for Their Origin

Le Qiao[1], James W. Head[2], Lionel Wilson[3], Jian Chen[1], Zongcheng Ling[1]

[1]Shandong Key Laboratory of Optical Astronomy and Solar-Terrestrial Environment, School of Space Science and Physics, Institute of Space Sciences, Shandong University, Weihai 264209, China.

[2]Department of Earth, Environmental and Planetary Sciences, Brown University, Providence, RI 02912, USA.

[3]Lancaster Environment Centre, Lancaster University, Lancaster LA1 4YQ, UK.

Contents of this file

Introduction

This supporting information contains additional figures and tables that are referred in the following sections of the main text: Figure S1 presents the titanium content map of Mare Tranquillitatis and is referred in the section 3; Figure S2 shows the areal density of mare domes in Mare Tranquillitatis and is referred in the sections 4.2, 5.3 and 6.4; Figure S3 presents additional statistics of morphometric parameters of Tranquillitatis domes and is referred in the sections 5.1 and 5.2; Figure S4 exhibits the distribution map of mare dome summit pit craters in Mare Tranquillitatis and is referred in the section 5.2; Figure S5 presents additional statistics of morphometric parameters of mare dome summit pit craters in Mare Tranquillitatis and is referred in the section 5.2; Figure S6 exhibits the frequency histogram of the average composition of Tranquillitatis domes and is referred in the section 5.3; Figure S7 shows the distribution map of other associated volcanic features in Mare Tranquillitatis and is referred in the section 6.2; Table S1 lists mare domes previously identified in Mare Tranquillitatis and is referred in section 4.

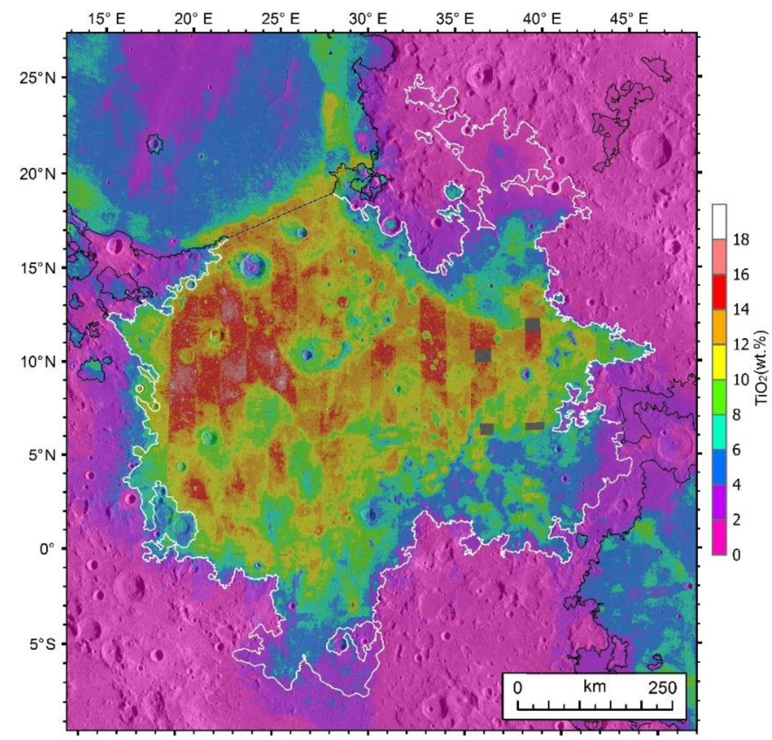

Figure S1. TiO_2 abundance of Mare Tranquillitatis calculated from Clementine UVVIS spectrometer data using the Lucey et al. (2000) algorithm.

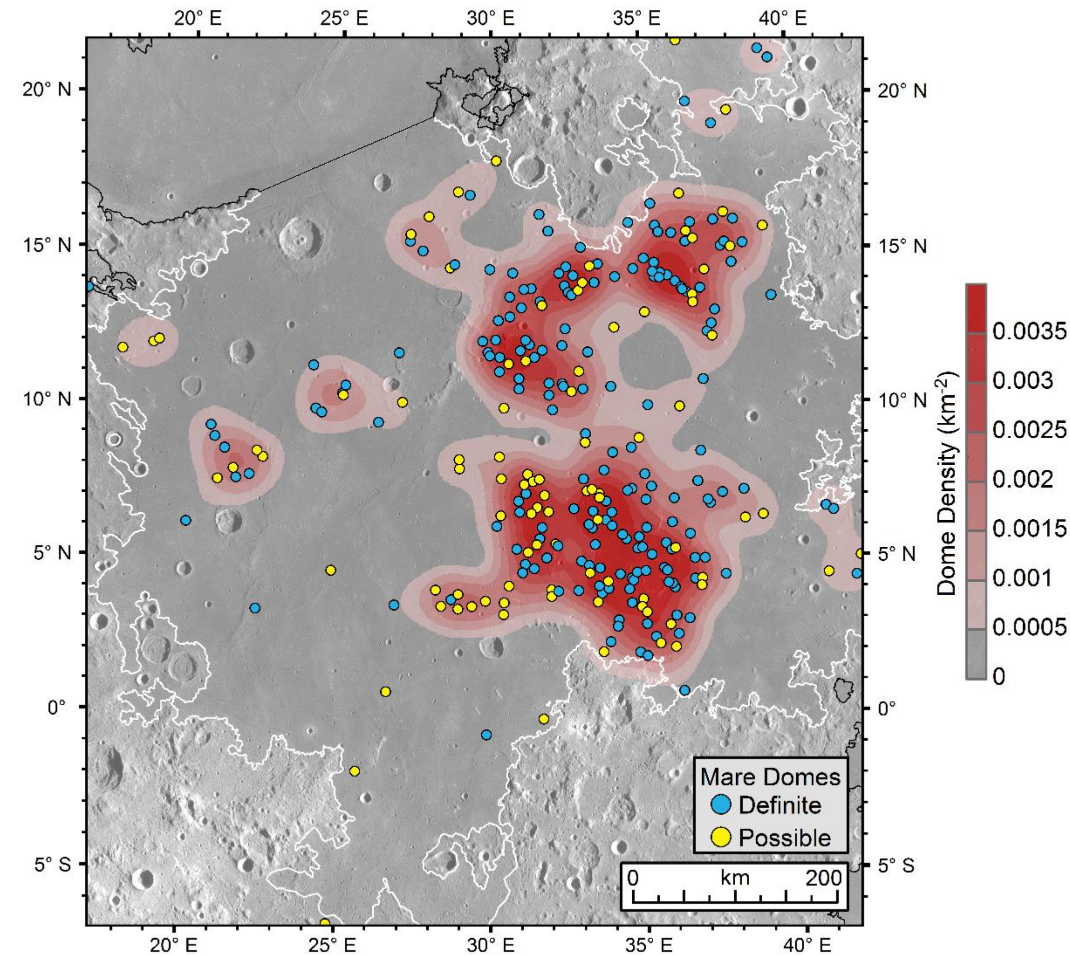

Figure S2. Areal density of identified dome features (marked by filled circles) in Mare Tranquillitatis, calculated in moving neighborhoods of radius 50 km.

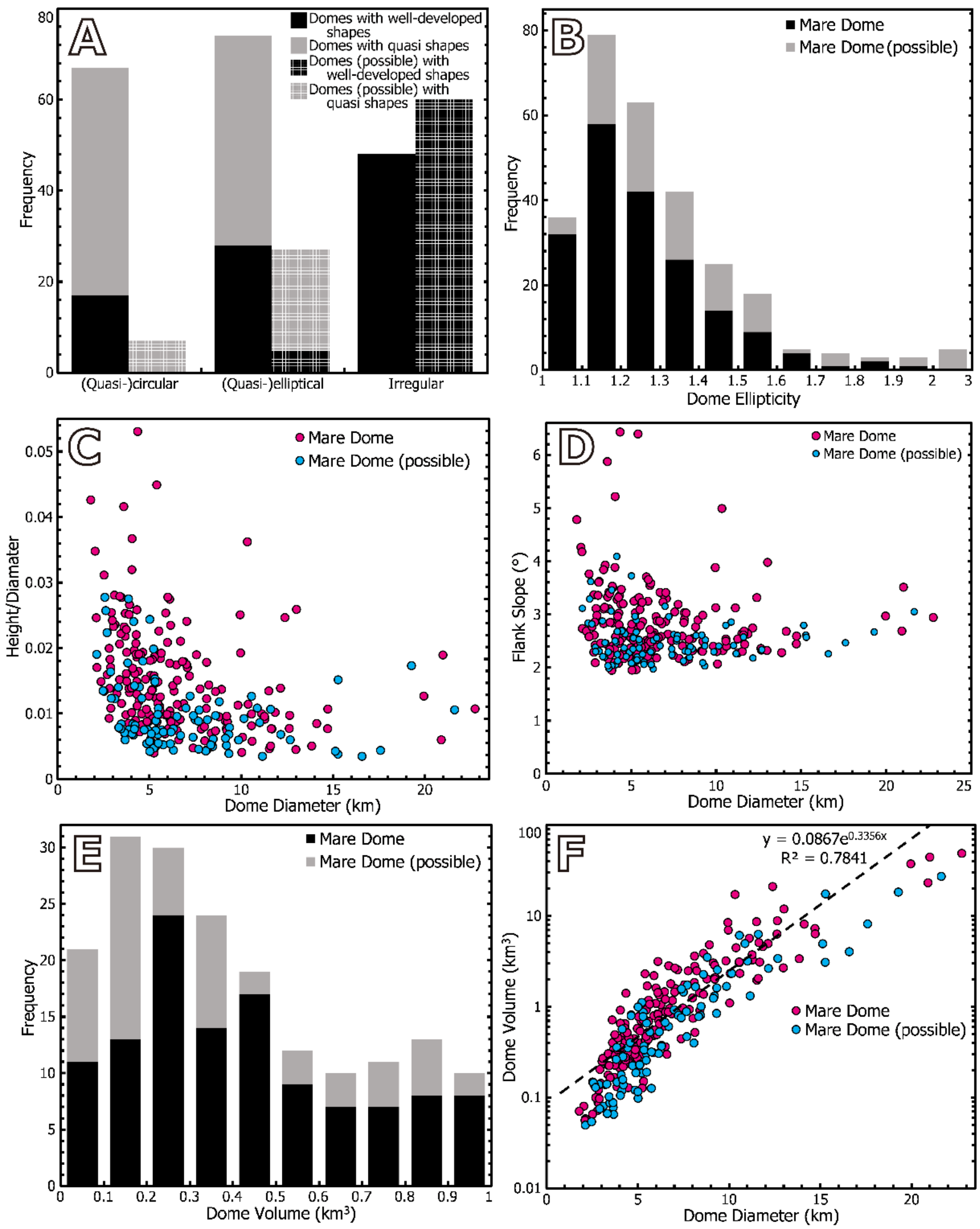

Figure S3. Additional statistics of morphometric parameters of mare domes in Mare Tranquillitatis: frequency histograms of (A) dome shape types, (B) dome base outline ellipticity and (E) dome volume (for domes less than 1 km^3 in volume), and plots of (C) dome height/diameter ratio, (D) flank slope (calculated from SLDEM2015 topography at a baseline of ~180 m) and (F) dome volume against dome base diameter.

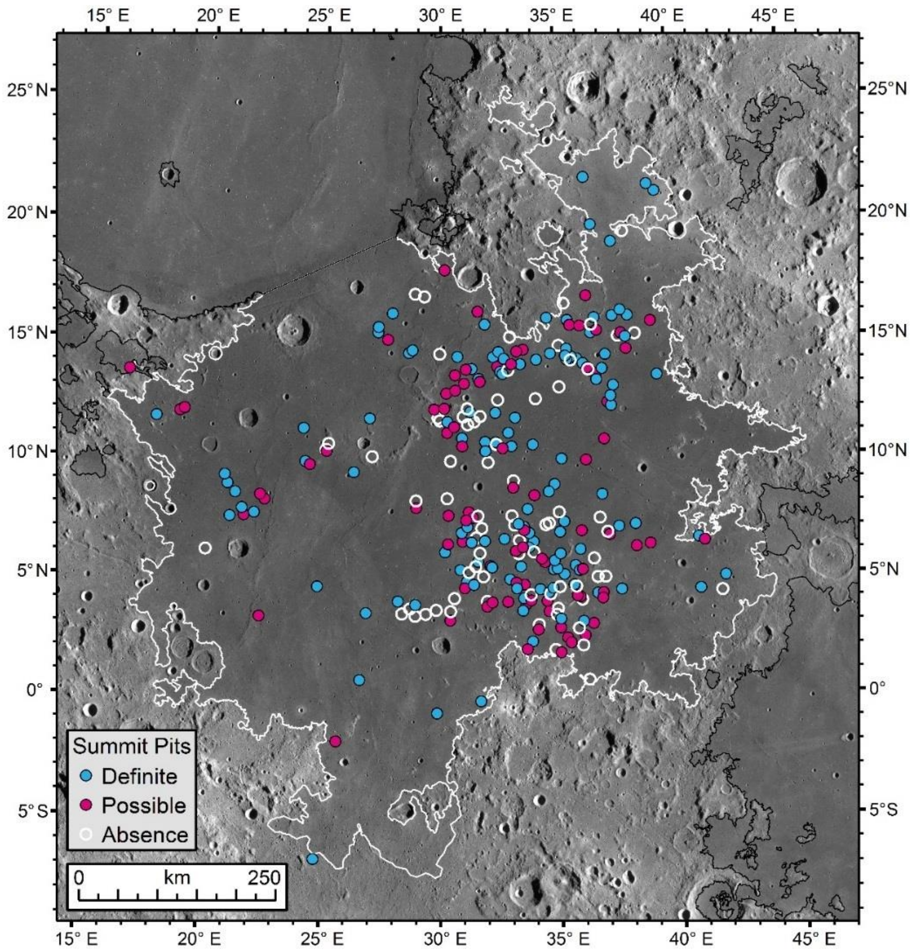

Figure S4. Spatial distribution of identified mare dome summit pit craters in Mare Tranquillitatis. Confirmed summit pits are marked with blue filled circles, possible pits are marked with magenta filled circles, and mare dome without summit pit are white circles.

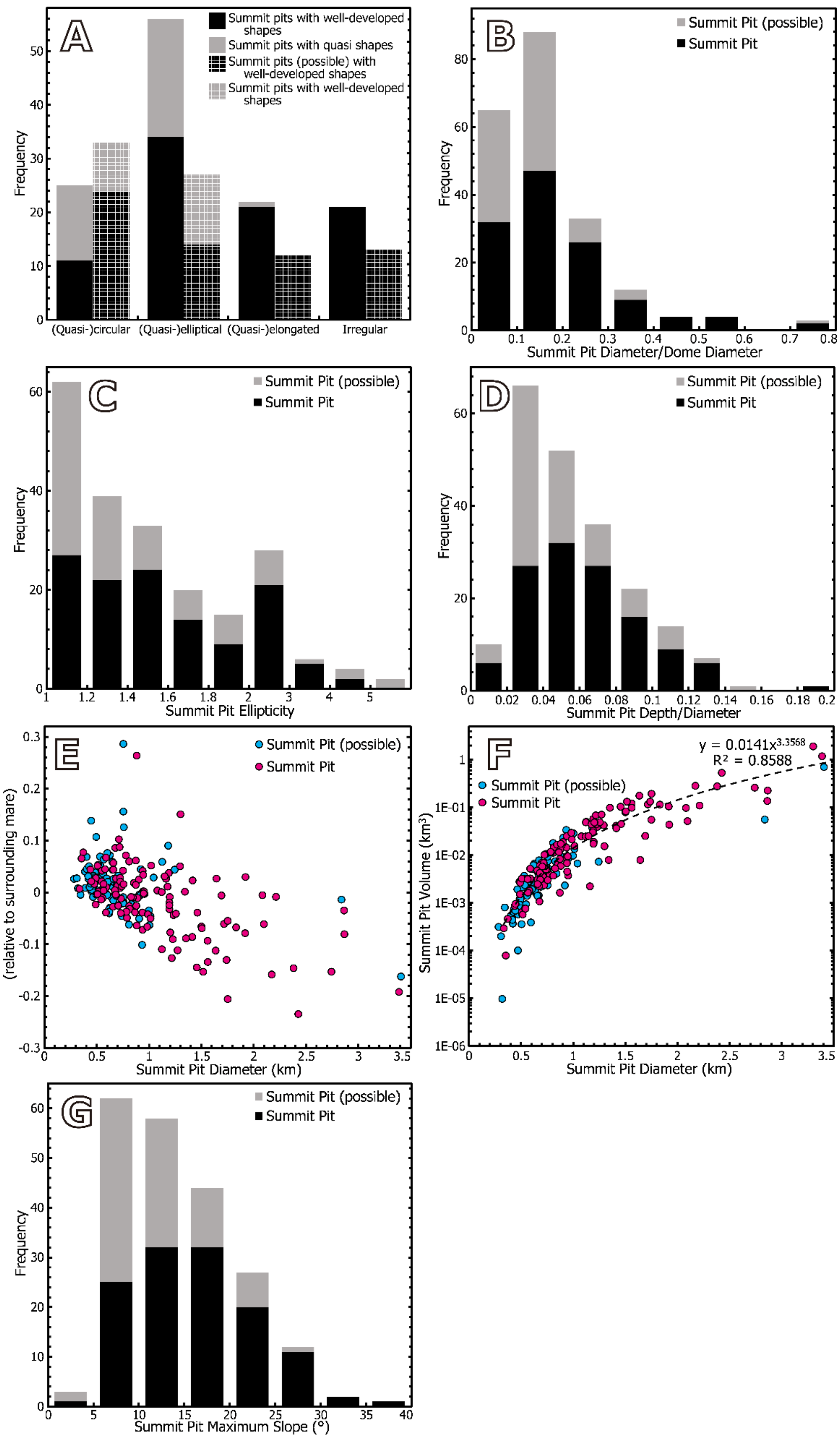
A
Summit pits with well-developed shapes
Summit pits with quasi shapes
Summit pits (possible) with well-developed shapes
Summit pits with well-developed shapes
Frequency
(Quasi-)circular
(Quasi-)elliptical
(Quasi-)elongated
Irregular
B
Summit Pit (possible)
Summit Pit
Summit Pit Diameter/Dome Diameter
C
Summit Pit Ellipticity
D
Summit Pit Depth/Diameter
E
Summit Pit Depth (km)
(relative to surrounding mare)
Summit Pit Diameter (km)
F
y = 0.0141x$^{3.3568}$
R² = 0.8588
Summit Pit Volume (km³)
G
Summit Pit Maximum Slope (°)

Figure S5. Additional statistics of the morphometric parameters of mare dome summit pit craters in Mare Tranquillitatis: frequency histograms of (A) summit pit shape type, (B) ratio of the summit pit diameter to the underlying dome base diameter, (C) summit pit rim outline ellipticity, (D) summit pit depth/diameter ratio and (G) the maximum topographic slope of the summit pit crater interior (calculated from SLDEM2015 topography at a baseline of ~180 m), and plots of (E) summit pit depth (relative to the surrounding mare) and (F) summit pit cavity volume against the summit pit diameter. Note that one pit 3.8 km in diameter is not plotted in panels E and F, and one pit 0.56 km deep is not plotted in panel E.

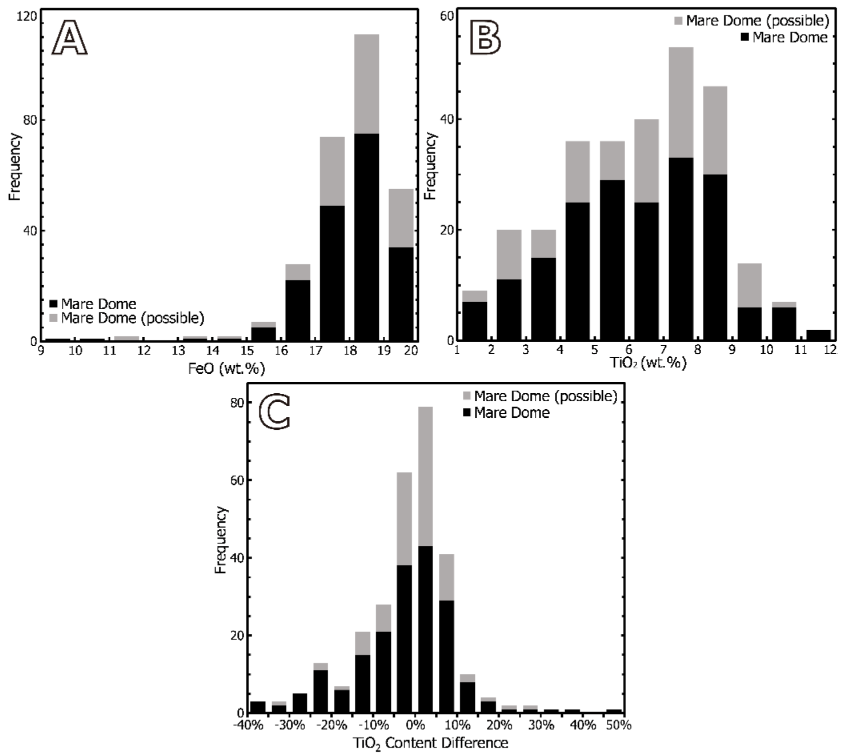

Figure S6. Frequency histogram of the average (A) FeO and (B) TiO_2 contents of Tranquillitatis domes, and (C) the TiO_2 content difference between those of mare domes and the surrounding mare surface (in percentage relative to mare TiO_2 content).

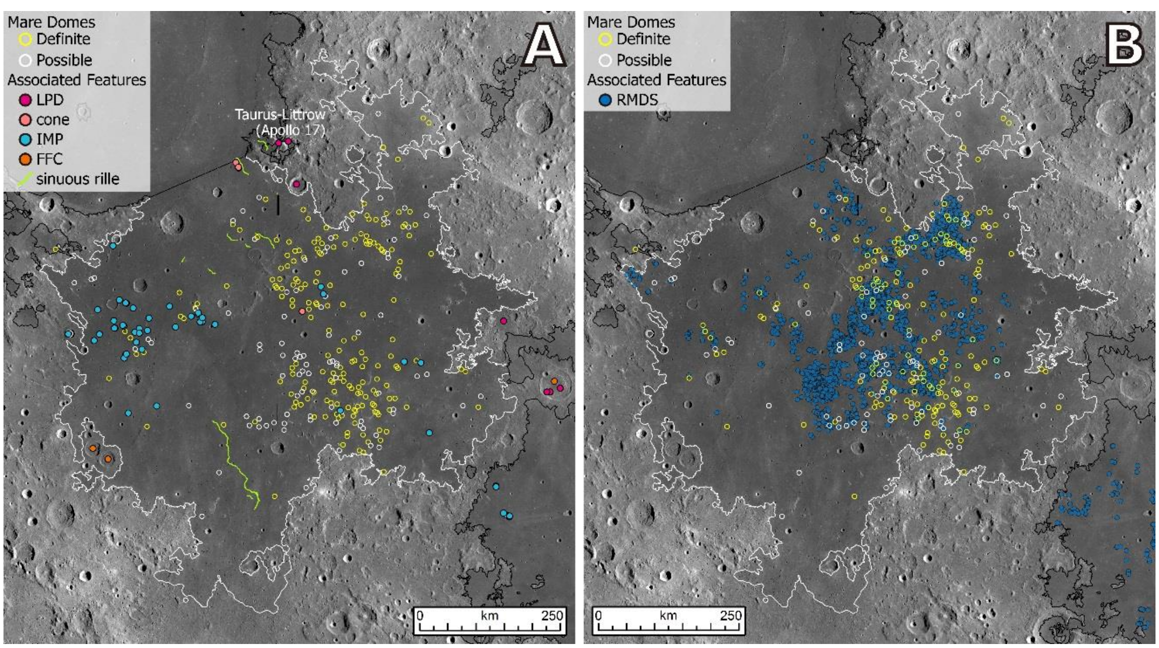

Figure S7. Spatial distribution of other associated volcanic features in Mare Tranquillitatis: (A) lunar pyroclastic deposits (LPDs), pyroclastic cones, Irregular Mare

Patches (IMPs), floor-fractured craters (FFCs) and sinuous rilles, and (B) ring-moat dome structures (RMDSs). The background map is a Kaguya TC morning image mosaic.

Table S1. A list of mare domes previously identified in Mare Tranquillitatis.

Dome name in this work	Lat [°]	Long [°]	Reliability[1]	Diameter (km)	Reference[2]	Dome name in previous works
Arago 1	6.14	20.03	A	12.4	HG80	Arago 1
Arago 2	7.55	21.56	A	21.0	HG80	Arago 2
Arago 3	8.53	21.20	A	12.6	HG80	Arago 3
Arago 4	8.93	20.89	A	9.1	HG80	Arago 4
Arago 5	9.27	20.76	A	7.2	HG80	Arago 5
Arago 6	11.28	24.12	A	5.6	HG80	Arago 6
Cauchy 1	7.22	38.31	A	8.9	HG80	Cauchy 1
Cauchy 2	7.52	36.76	A	9.9	HG80	Cauchy 2
Cauchy 4	8.50	36.93	A	9.2	HG80	Cauchy 4
Cauchy 5	7.14	37.60	A	5.7	HG80	Cauchy 5
Jansen 1	11.55	31.44	A	12.1	HG80	Jansen 1
Jansen 2	11.11	30.28	A	6.3	HG80	Jansen 2
Jansen 3	11.77	30.98	A	4.3	HG80	Jansen 3
Jansen 4	11.96	31.27	A	4.8	HG80	Jansen 4
Jansen 5	12.48	32.46	A	6.1	HG80	Jansen 5
Jansen 6	11.94	32.35	A	14.1	HG80	Jansen 6
Jansen 7	11.76	33.21	A	11.5	HG80	Jansen 7
Jansen 8	10.62	33.97	A	6.7	HG80	Jansen 8
Maskelyne 1	2.31	33.89	A	7.8	HG80	Mashelyne 1
Sinas 1	10.53	33.05	A	8.1	HG80	Sinas 1
Sinas 2	10.72	32.35	A	4.3	HG80	Sinas 2
Sinas 3	10.71	31.92	A	6.5	HG80	Sinas 3
Vitruvius 1	14.21	35.88	A	6.7	HG80	Vitruvius 1
Vitruvius 2	14.29	35.65	A	6.1	HG80	Vitruvius 2
Vitruvius 3	14.76	35.10	A	9.2	HG80	Vitruvius 3
Vitruvius 4	14.44	34.74	A	6.0	HG80	Vitruvius 4
Vitruvius 5	14.16	34.17	A	10.1	HG80	Vitruvius 5
Vitruvius 6	14.00	33.47	A	7.5	HG80	Vitruvius 6
Vitruvius 7	14.30	32.29	A	7.0	HG80	Vitruvius 7
Vitruvius 8	14.53	32.51	A	6.8	HG80	Vitruvius 8
Vitruvius 9	13.89	32.47	A	5.0	HG80	Vitruvius 9
Vitruvius 10	14.23	32.76	A	11.3	HG80	Vitruvius 10
Vitruvius 11	15.80	35.50	A	5.9	HG80	Vitruvius 11
Vitruvius 12	15.15	37.69	A	5.2	HG80	Vitruvius 12
Vitruvius 13	13.43	39.38	A	13.0	HG80	Vitruvius 13
Aryabhata 1	7.23	34.48	A	4.8	TH13	
Aryabhata 10	6.20	35.95	A	11.5	TH13	
Aryabhata 16	5.12	35.25	A	6.5	TH13	

Aryabhata 18	**5.36**	**34.79**	**A**	**4.3**	**TH13**
Aryabhata 2	**7.28**	**34.61**	**A**	**3.7**	**TH13**
Aryabhata 20	**5.65**	**34.46**	**A**	**5.0**	**TH13**
Aryabhata 22	**6.05**	**33.93**	**A**	**5.9**	**TH13**
Aryabhata 23	**6.26**	**33.76**	**A**	**5.4**	**TH13**
Aryabhata 26	**6.02**	**33.33**	**A**	**4.2**	**TH13**
Aryabhata 27	**6.50**	**33.97**	**A**	**10.6**	**TH13**
Aryabhata 28	**6.58**	**33.34**	**A**	**5.5**	**TH13**
Aryabhata 3	**6.90**	**35.06**	**A**	**8.0**	**TH13**
Aryabhata 30	**6.87**	**33.76**	**A**	**3.4**	**TH13**
Aryabhata 35	**7.57**	**33.00**	**A**	**10.6**	**TH13**
Aryabhata 36	**7.89**	**33.70**	**A**	**5.1**	**TH13**
Aryabhata 4	**7.35**	**35.24**	**A**	**3.9**	**TH13**
Carrel 3	**9.44**	**26.31**	**A**	**6.1**	**TH13**
Carrel 8	**9.88**	**24.25**	**A**	**8.1**	**TH13**
Jansen 10	**14.57**	**28.77**	**A**	**4.6**	**TH13**
Jansen 12	**14.34**	**30.75**	**A**	**10.3**	**TH13**
Jansen 23	**11.74**	**29.91**	**A**	**5.5**	**TH13**
Jansen 24	**11.62**	**29.97**	**A**	**2.1**	**TH13**
Jansen 25	**11.57**	**30.27**	**A**	**3.6**	**TH13**
Jansen 29	**11.78**	**31.72**	**A**	**8.4**	**TH13**
Jansen 9	**14.47**	**28.67**	**B**	**3.9**	**TH13**
Maraldi 1	**21.77**	**36.22**	**B**	**12.2**	**TH13**
Maraldi 2	**19.79**	**36.55**	**A**	**6.3**	**TH13**
Maraldi 4	**19.12**	**37.46**	**A**	**6.2**	**TH13**
Maraldi 5	**21.45**	**39.07**	**A**	**6.9**	**TH13**
Maraldi 6	**21.11**	**39.44**	**A**	**7.6**	**TH13**
Maskelyne 11	**3.05**	**34.14**	**A**	**11.9**	**TH13**
Maskelyne 15	**-0.66**	**29.71**	**A**	**22.8**	**TH13**
Menzel 11	**4.69**	**35.64**	**A**	**6.2**	**TH13**
Menzel 16	**3.99**	**34.51**	**A**	**4.4**	**TH13**
Menzel 21	**2.94**	**35.15**	**A**	**14.7**	**TH13**
Menzel 22	**3.14**	**36.02**	**A**	**8.6**	**TH13**
Menzel 23	**3.05**	**36.44**	**A**	**4.4**	**TH13**
Menzel 6	**5.01**	**37.05**	**A**	**13.8**	**TH13**
Sinas 12	**9.06**	**33.11**	**A**	**4.0**	**TH13**
Sinas 5	**10.50**	**30.94**	**A**	**7.8**	**TH13**
Sinas 6	**10.78**	**30.98**	**A**	**12.6**	**TH13**
Sinas 7	**9.86**	**32.08**	**A**	**2.7**	**TH13**
Theophilus 1	**-6.80**	**24.58**	**B**	**86.9**	**TH13**
Vitruvius 23	**15.97**	**37.49**	**A**	**6.1**	**TH13**
Vitruvius 25	**15.99**	**38.12**	**A**	**3.6**	**TH13**
Vitruvius 32	**14.62**	**35.42**	**A**	**4.9**	**TH13**

Vitruvius 33	**14.32**	**35.40**	**A**	**4.3**	**TH13**	
Vitruvius 34	**14.16**	**35.42**	**A**	**4.3**	**TH13**	
Vitruvius 35	**14.15**	**35.61**	**A**	**3.8**	**TH13**	
Vitruvius 36	**13.96**	**36.22**	**A**	**9.2**	**TH13**	
Vitruvius 39	**13.62**	**36.51**	**A**	**7.0**	**TH13**	
Vitruvius 43	**13.04**	**37.45**	**A**	**6.5**	**TH13**	
Vitruvius 47	**13.01**	**35.21**	**B**	**6.2**	**TH13**	
Vitruvius 48	**14.62**	**33.59**	**A**	**6.0**	**TH13**	
Vitruvius 54	**15.14**	**33.00**	**A**	**4.3**	**TH13**	
Vitruvius 57	**17.89**	**30.18**	**B**	**21.6**	**TH13**	
Wallach 12	**3.86**	**33.57**	**A**	**10.6**	**TH13**	
Zahringer 1	**6.64**	**40.99**	**A**	**6.7**	**TH13**	
Zahringer 4	**4.33**	**41.91**	**A**	**5.6**	**TH13**	
Arago 9	**7.71**	**22.05**	**A**	**3.7**	**Wöhler et al.**	**A1**
Carrel 2	**10.11**	**27.08**	**B**	**2.6**	**Wöhler et al.**	**Ca1**
Cauchy 10	**10.00**	**35.19**	**A**	**5.2**	**Wöhler et al.**	**C10**
Cauchy 12	**10.86**	**37.02**	**A**	**20.9**	**Wöhler et al.**	**C11**
Vitruvius 40	**13.57**	**36.71**	**B**	**5.3**	**Wöhler et al.**	**NTA5**
Vitruvius 45	**12.38**	**37.16**	**A**	**5.3**	**Wöhler et al.**	**C12**

[1]Mare dome or summit pit crater identification reliability: A = definite dome structures; B = possible mare dome; C = questionable dome identifications.
[2]Souce references for previous mare dome identifications: HG80: Head & Gifford (1980); TH13: Tye & Head, 2013; Wöhler et al.: Wöhler et al., 2006, 2007, 2009.